Converting Vertical Vibration of a Texture Ratchet into Horizontal Drop Motion

Yan Dong

A thesis

Submitted in partial fulfillment of the

Requirements for the degree of

Master of Science in Bioengineering

University of Washington

2012

Committee:

Karl F. Böhringer

Gerald H. Pollack

Program Authorized to Offer Degree:

Master Program of the Department of Bioengineering

University of Washington

Graduate School

This is to certify that I have examined this copy of a master's thesis by

Yan Dong

and have found that it is complete and satisfactory in all respects,

and that any and all revisions required by the final

examining committee have been made.

Committee Members:

Karl F. Böhringer

Gerald H. Pollack

In presenting this thesis in partial fulfillment of the requirements for a master's degree at the University of Washington, I agree that the Library shall make its copies freely available for inspection. I further agree that extensive copying of this thesis is allowable only for scholarly purposes, consistent with "fair use" as prescribed in the U.S. Copyright Law. Any other reproduction for any purposes or by any means shall not be allowed without my written permission.

University of Washington

Abstract

Converting Vertical Vibration of a Texture Ratchet into Horizontal Drop Motion

Yan Dong

Chair of the Supervisory Committee:

Professor: Karl F. Böhringer

Bioengineering and Electrical Engineering

A texture ratchet is an anisotropic, periodic, microstructured surface that propels drops when vibrated with a sinusoidal signal at certain frequencies and amplitudes. For each input frequency near the resonant frequency of a drop, there is a threshold amplitude beyond which the drop starts to move. In this thesis, we study the parameters that initiate drop motion and reveal a general relationship between the input frequency and threshold amplitude among drops with different volumes, densities, viscosities and surface tensions. We propose a compact model that captures the essential features of the system to describe how a pure vertical vibration results in horizontal drop motion. This model provides an intuitive understanding of the underlying physics and explains how the surface asymmetry is the key for lateral drop motion.

TABLE OF CONTENTS

LIST OF FIGURES

LIST OF TABLES

Chapter 1

Introduction and Overview

With the rapid advance of different fabrication techniques in microelectromechanical systems (MEMS), various microfluidic devices have been developed to manipulate and analyze liquids of very small quantities. Such devices are called Lab-on-a-Chip devices [1] where all experimental setups in a traditional lab are transformed into a microscale network composed of channels, valves [2], pumps [3], mixers [4], etc. The entire experimental procedure can be executed within this network to enhance efficiency and mobility as well as reducing sample and reagent size. These low-cost, easy-to-use, portable and disposable devices can be used as a convenient tool to carry out biochemical analysis and disease diagnostics such as DNA sequencing [5], polymerase chain reaction (PCR) [6], electrophoresis [7], DNA separation [8], high throughput screening in drug development [9, 10], and point-of-care detection of toxins and pathogens [11, 12]. In most cases, these microfluidic devices handle continuous fluid where several streams of liquid are moved and manipulated simultaneously in the microscale network.

Recently, another rapidly expanding collection of microfluidic devices has been designed and developed. These so-called drop-based microfluidic devices are capable of handling discrete drops [13-15] instead of continuous fluids. They are of great interest because they 1) digitize the fluid into discrete drops so that a group of drops containing different

chemicals can be manipulated in a designated sequence, 2) further decrease the required amount of sample and reagent, and 3) make it possible for massively parallel operation. A detailed literature review will be given in the remaining part of this chapter, followed by the specific aims of this work.

1.1 Literature review on drop microfluidic devices

Two general types of drop microfluidic devices have been developed in the past decade to generate, transport, merge and analyze drops. One comprises a series of microchannels in a closed system where discrete drops are generated and manipulated in a different continuous fluid (i.e., two-phase emulsion) [16, 17]. For example in a flow-focusing microfluidic device (Figure 1), a stream of oil is "focused" at the orifice by two streams of water from either side; the oil phase is then broken into discrete drops because of capillary instability. The other type, on the contrary, is an open system where small sessile drops are moved in air on a usually hydrophobic surface [18, 19].

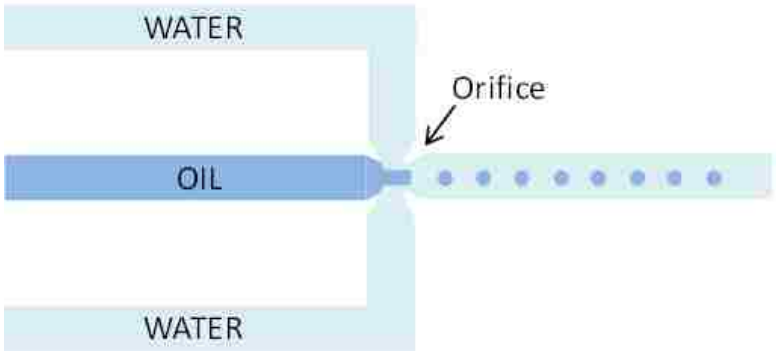

Figure 1. Top view schematic of a closed system flow-focusing microfluidic device. Oil is "focused" at the orifice by two water streams on either side so that discrete oil drops are generated in the downstream.

Advantages of the open system include 1) easy and precise control of drop motion – a sessile drop can be moved from one spot to a specific target – and 2) prevention of dilution by diffusion or contamination across the two-phase boundary.

Many of these open system devices have been developed recently. Sessile drops are transported by a surface energy gradient created by electrowetting [20-22], superparamagnetism [23], Leidenfrost effect [24, 25] or mechanical agitation [26-28]. In the case of electrowetting, a drop is sandwiched between two electrodes that changes polarity at a certain frequency. When a voltage is applied between the two electrodes, the solid-liquid interface energy is reduced, which leads to a reduction in contact angle and thus a spreading of the liquid on the substrate. With careful design of the electrodes and input voltage, a net drop motion can be achieved with an average velocity exceeding 10 cm/s. For superparamagnetism, a drop containing paramagnetic particles is moved on a ratchet-structure superhydrophobic surface with carefully controlled magnetic field. For the Leidenfrost effect, a drop performs self-propelled motion on a hot surface with ratchetlike topography. The vapor flow between the solid and liquid exerts a viscous force that drives drop motion. As for mechanical agitation, the substrate on which the sessile drop is placed can vibrate in a certain manner so that an asymmetric contact angle is created along the three phase contact line of the sessile drop. This asymmetry results in a hydrophobic gradient around the drop footprint, thus causing a net drop motion in the direction along with the decreasing hydrophobic gradient.

In all these cases, the drop does not move at a constant speed as it seemingly is. Instead, it moves in a ratcheting fashion. For example under mechanical agitation, slow motion videos show that the leading and trailing edges of the drop move back and forth in each oscillation cycle and a net forward motion can be achieved because of surface energy asymmetry [29].

1.2 Ratchet motion in biology

Such ratchet motion appearing in the drop microfluidic device can also be found in biology. For example, a shorebird can move a water drop from the tip of its beak to its mouth in a stepwise ratcheting fashion by repeatedly opening and closing its beak. Another example is the actin bundle [30]. Its polymerization provides the force that can propel a bacterium through the cell surface in a ratchet fashion [31].

1.3 Texture ratchet

A texture ratchet is a new type of drop microfluidic device developed in recent years [32]. It is an anisotropic microstructured surface that can create a hydrophobic gradient and propel a drop when vertically vibrated with a square or sinusoidal signal. Usually to create a hydrophobic gradient, surfaces can be treated by either chemical deposition [33] that gradually changes the surface material property, or by microstructure design [26, 32] that changes the surface morphology. Shastry et al. introduced a texture ratchet with periodic micropillars in different sizes, creating a repeating pattern of local hydrophobic gradients that can transport drops with mechanical agitation [34]. Duncombe et al. built on this idea and developed similar ratchets with a track of straight

and curved rungs, along which drops can move under a pure vertical vibration [29, 35]. Figure 2 shows the illustration of their respective devices. In all cases, a drop sits in its "fakir" state [36] on the hydrophobic surfaces and moves in the longitudinal direction along the designated track. The areas on either side of the track are more hydrophobic than the track itself, thus creating a surface potential well that keeps the drop confined to the track. In order to initiate the motion of a drop on such texture ratchets, a certain combination of input frequency and amplitude of vibration is required. For each input frequency tested, there is a threshold amplitude of vibration, beyond which the drop starts to move. In this thesis, the original data set of this combination is drawn from the rung/pillar device shown in Figure 2b. A theoretical study will be conducted in chapter 3 and 4 to learn the underlying physics behind the drop motion on this texture ratchet.

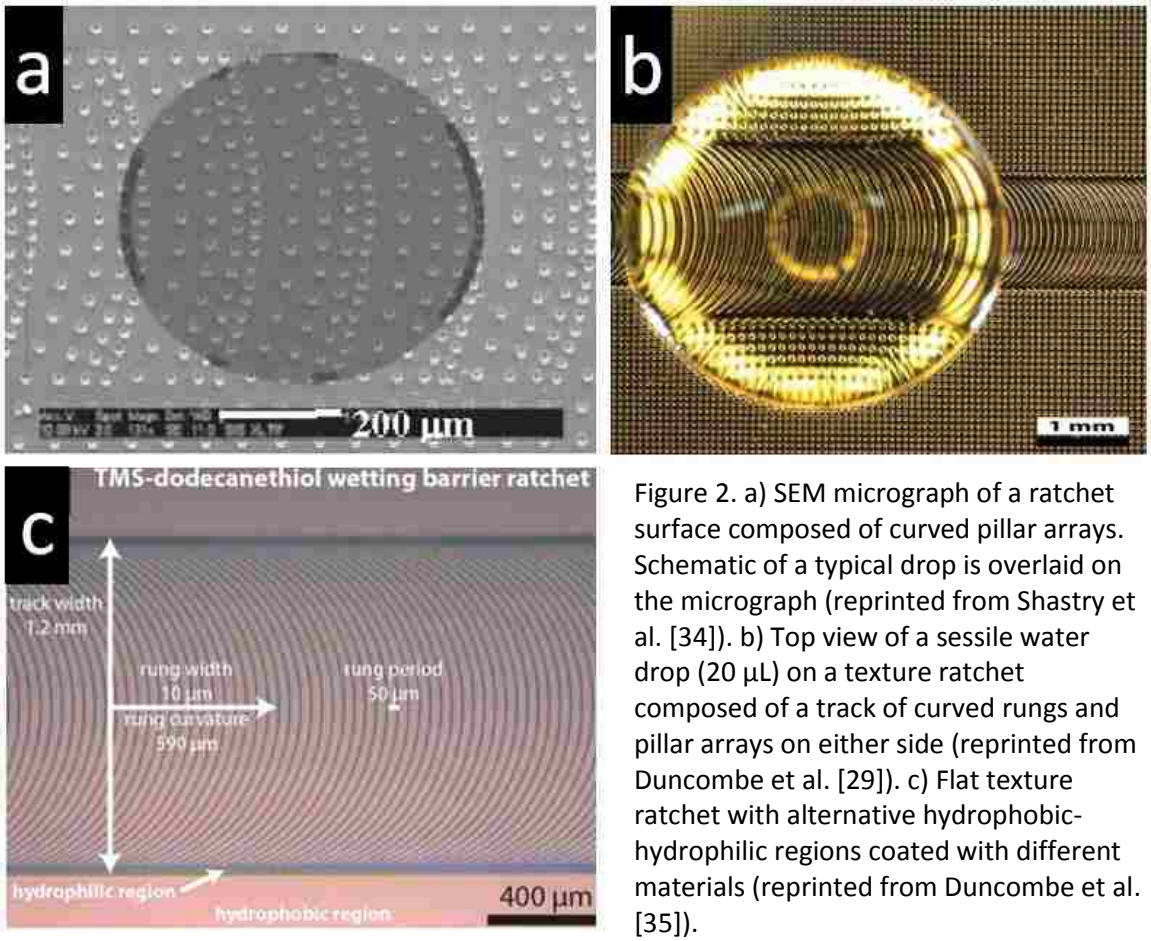

Figure 2. a) SEM micrograph of a ratchet surface composed of curved pillar arrays. Schematic of a typical drop is overlaid on the micrograph (reprinted from Shastry et al. [34]). b) Top view of a sessile water drop (20 µL) on a texture ratchet composed of a track of curved rungs and pillar arrays on either side (reprinted from Duncombe et al. [29]). c) Flat texture ratchet with alternative hydrophobic-hydrophilic regions coated with different materials (reprinted from Duncombe et al. [35]).

1.4 Theoretical work for open system drop microfluidic devices

Although the phenomenon of a drop moving on a textured ratchet has been characterized empirically, no theoretical work has been done to explain the underlying physics. However, several models have been proposed to describe the mechanism of drop motion in other similar systems, often modeling the drop as a sliding or rolling solid. Noblin's model [37] was based on a smooth substrate and demonstrated that the combination of horizontal and vertical vibrations can create a force asymmetry, thus causing a net drop motion. Malvadkar et al. [38] proposed a model that described the

pin-release mechanism of a ratchet by analyzing the contact angles at a microscopic level. Daniel [27, 39], Buguin [28], Mettu [40, 41] and their co-workers investigated similar systems and described how horizontal vibration can overcome the contact angle hysteresis and cause a net drop motion. Goohpattader et al. studied drift of a sphere during stochastic rolling on a patterned substrate [42, 43]. All these models help to better understand the mechanism of drop motion on a vibrating surface, but none of them can explain, in the case of a pure vertical vibration, how a sessile drop is propelled across a horizontal substrate.

1.5 Specific aims

In this paper, we propose a model that shows how a vibration applied perpendicularly to the anisotropic texture ratchet will induce a lateral drop motion on horizontal and inclined substrates. The scope of this work includes two specific aims. First, we generalize the condition of drop motion by non-dimensionalizing the data with different drop characteristics (i.e., volume, density, viscosity, surface tension). We expect a general relationship between input frequency and threshold amplitude of vibration across drops with different properties. Second, we introduce a compact model that captures the important features of a moving drop to describe the mechanism behind drop motion on a texture ratchet. A good agreement is expected between the simulation results of the model and the experimental data.

Chapter 2

Experimental Setup and Observations

In this chapter, the original experimental setup by Duncombe et al. [29] is presented in order to clarify how the experiments were conducted and what observations have been made to study the drop motion.

2.1 Experiment

2.1.1 Fabrication of texture ratchet

The characteristic of the texture ratchet is shown in Figure 3, with a sessile drop sitting in the middle. The texture ratchet is fabricated by photolithography and etching techniques on a silicon wafer to create the designated surface features. A thin coating of fluoro-octyl-trichloro-silane (FOTS, Sigma) is then applied by vapor deposition to the surface to make it more hydrophobic. It is composed of a track of curved rungs in the middle and sparse pillars on either side. Because of its overall hydrophobic property, a sessile drop will bead up on the surface and remain in "fakir" state. Since the pillars are relatively more hydrophobic, it creates a surface potential well that keeps the drop confined to the track.

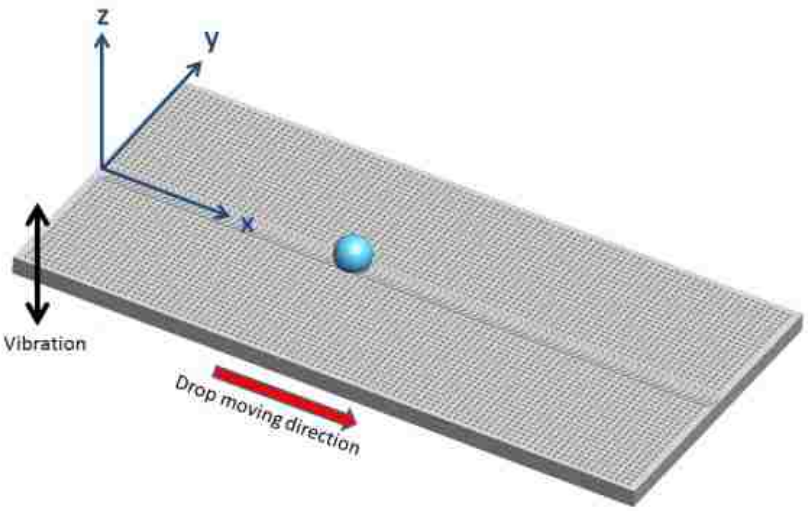

Figure 3. Schematic of texture ratchet in three-dimensional coordinates. A central track of curved rungs is delimited by sparse arrays of pillars on either side. Typical dimensions are about 1 mm for track width, and tens of μm for rung and pillar width and height.

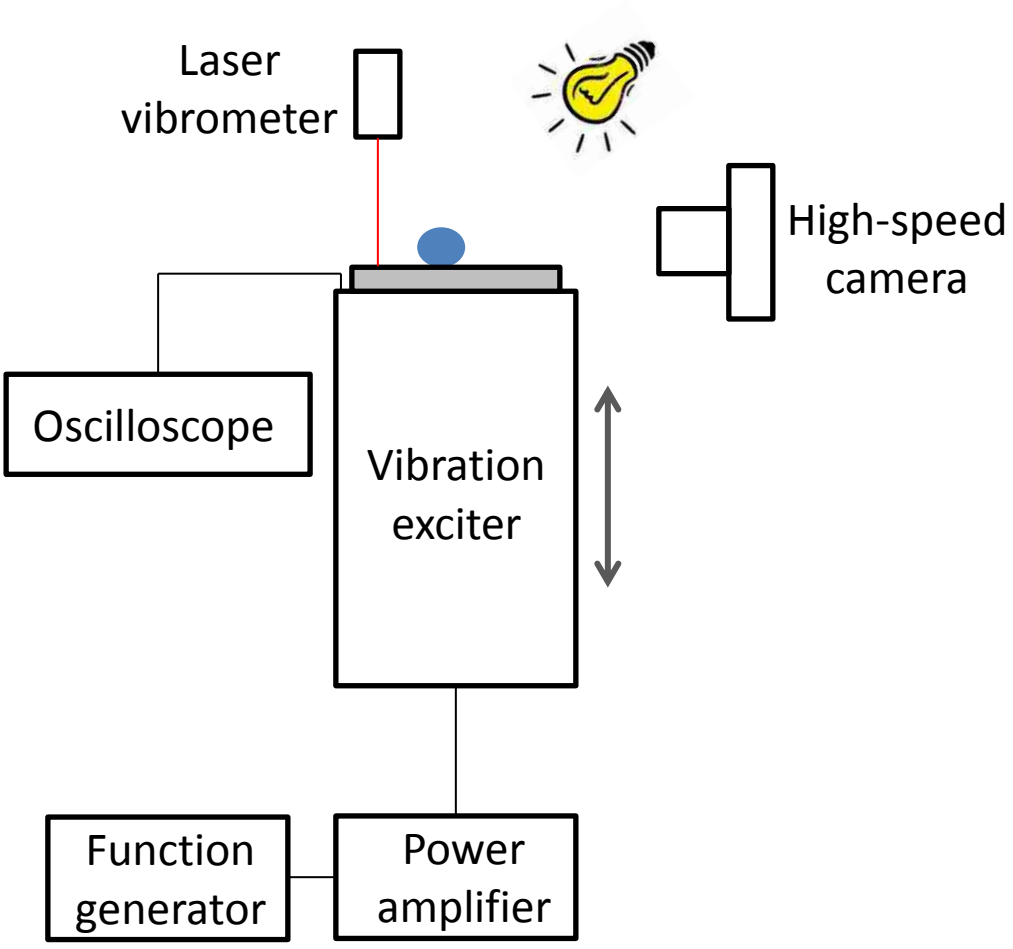

Figure 4. Schematic of experimental setup.

2.1.2 Experimental setup

A detailed experimental setup is shown in Figure 4. A sinusoidal signal is applied from the function generator and amplified by the power amplifier. The texture ratchet (shown in grey) is tightly attached to a vibration exciter and vibrates vertically in response to the input signal. An oscilloscope is attached to the platform of the exciter to monitor the signal transfer. The acceleration (or amplitude of vibration) of the texture ratchet is measured by a laser vibrometer. A high speed camera is placed on the side of the substrate to take pictures and videos of the moving drop.

2.2 Observations

2.2.1 Relationship between input frequency and threshold amplitude of vibration

The motions of a total of four drops were characterized in the previous experiment [29]. Three water drops of 5 µL, 8 µL, 13 µL and a 50% v/v glycerol-water mixture drop with 8 µL were tested under a range of frequencies and amplitude of vibration. The relationships between these two input factors are shown in Figure 5. For each input frequency, there is a threshold amplitude of acceleration of the substrate beyond which the drop starts to move. For example, the threshold amplitude of vibration for a 13 µL water drop at 150 rad/s is around 3.5 *g*, where *g* is the gravitational acceleration. For each drop, the minimum threshold amplitude occurs around the drop's resonance frequency, indicated in Figure 5 by the blue dotted lines. In the first case where three water drops are compared, as the volume gets larger, the resonance frequency decreases as well as the threshold amplitude of vibration. For water and glycerol drop

comparison, as the viscosity increases, the resonance frequency decreases but the threshold amplitude of vibration increases. In sum, drops with smaller volume and larger viscosity require larger amplitude of vibration because of the reduced inertia and increased damping, respectively.

2.2.2 Ratchet motion of a sessile drop

A general understanding of why a sessile drop moves on a texture ratchet is that the pin-release forces at the leading and trailing edges of the drop are asymmetric so that a net drop motion occurs in each oscillation cycle. Therefore, the displacements of the two edges and the center of mass are used to represent the drop motion. Figure 6 shows a typical displacement curve of the leading edge, trailing edge and the center of mass. In general, all three points move forward under vibration, but there is a clear oscillation at the leading and trailing edges. In addition, a clear phase shift between the two edges occurs in each oscillation cycle, indicating an asymmetric motion between the two edges. Moreover, the lateral movement of the trailing edge is larger than that of the leading edge, meaning that there is less resistance for the motion of the trailing edge. In other words, the pin-release force at the trailing edge is in general smaller than that at the leading edge.

These data and observations will be used as the raw data and references for further analysis in chapter 3 and 4.

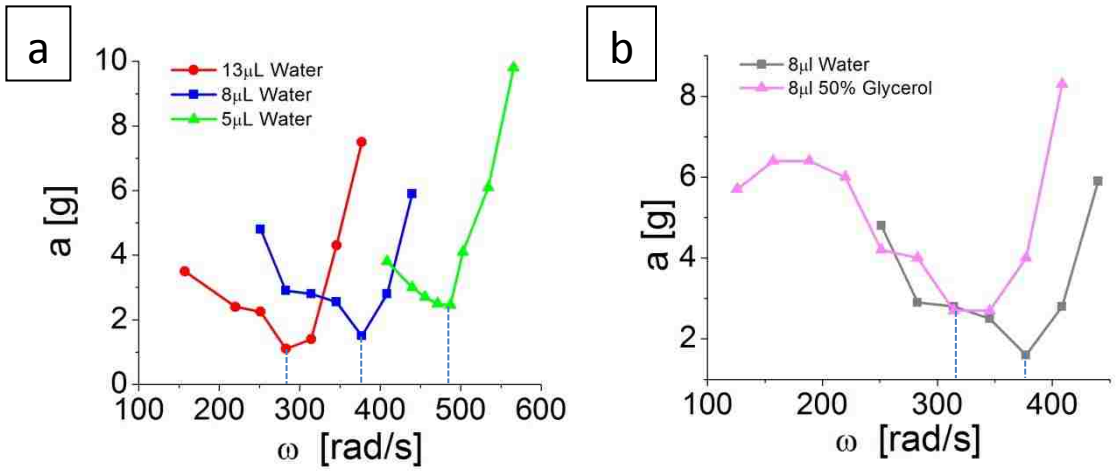

Figure 6. a) Relationship between angular frequency and threshold amplitude of vibration for three water drops with different volumes. b) Comparison between a water drop and a 50% v/v glycerol drop with same volume (reprinted from Dumcombe et al.'s paper [29]).

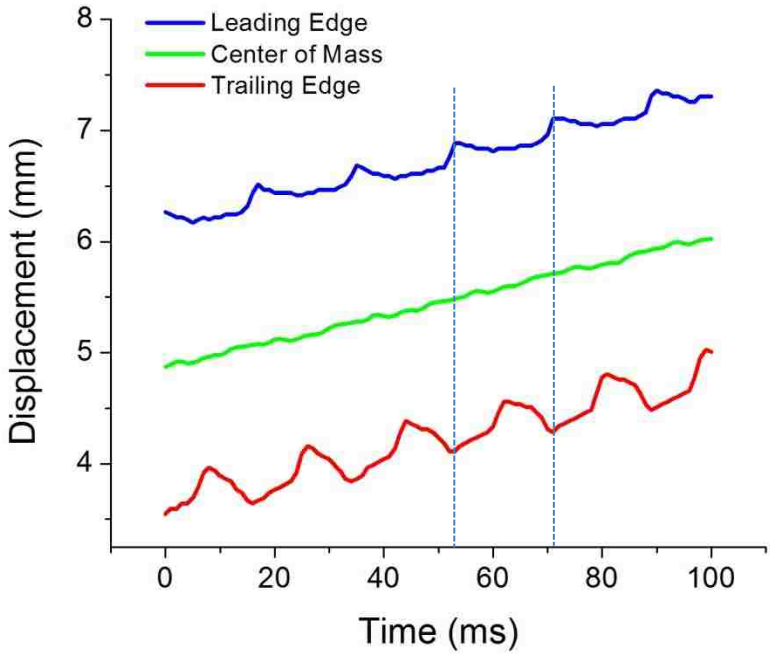

Figure 5. The displacement of the leading edge (blue), trailing edge (red) and center of mass (green) over time. Dotted lines capture the drop motion in one oscillation cycle (reprinted from Dumcombe et al.'s paper [29]).

Chapter 3

Non-dimensionalization of Drops with Different Characteristics

The experimental characterization of drop motion on texture ratchets in the previous chapter indicates that although the relationship between input frequency and amplitude of threshold acceleration is different among drops with different properties, there appears to be a general relationship between these two entities as the shapes of all curves are similar (see Figure 5). In order to generalize this relationship, angular frequency ω and amplitude of threshold acceleration a are non-dimensionalized to factor out the differences in drop properties.

3.1 Non-dimensionalization factors

We hypothesize that two non-dimensionalization factors, ω^* and a^*, can be chosen such that the relationship between ω/ω^* and a/a^* is identical across different drops. For this general relationship to hold, ω^* must be proportional to the resonance frequency of the drop and a^* must be proportional to the amplitude of threshold acceleration at resonance. Even though an exact analytical expression for the resonance frequency and threshold acceleration of an oscillating sessile drop on a textured surface may be difficult to obtain, these proportionalities allow us to express the scaling of the resonance frequency with respect to basic drop properties such as volume, density and surface tension. Furthermore, with an input signal $z(t) = Z\sin(\omega t)$, where Z is the amplitude of displacement, we can infer that a^* scales with $Z\omega^{*2}$.

In this work, the sessile drop is modeled as a mass-spring system, with viscous damping neglected for now. Viscous effects are measured by the Reynolds number

$$Re = \sqrt{\rho\gamma R_c}/\mu$$

where ρ is drop density, γ is surface tension, R_c is radius of curvature and μ is viscosity [44].

All drops tested in this case are nearly spherical because of the following two reasons.

1) All drop radii $R = \sqrt[3]{3V/4\pi}$ (V is drop volume) are smaller than the capillary length of the respective liquid (see Table 1). Capillary length is given by

$$Ca = \sqrt{\gamma/\rho g}$$

where g is gravitational acceleration.

2) The surface of the supporting substrate is highly hydrophobic which makes the drop beads up into a nearly spherical shape.

As a result, the radius of curvature R_c can be approximated by the spherical drop radius R, which gives

$$Re = \sqrt{\rho\gamma R}/\mu$$

By calculation, the minimum Re in this work is 37.1 for a 50% v/v glycerol drop (see Table 1). According to Wilkes and Basaran [45], viscous effects are negligible for sessile drops with $Re > 20$. Therefore, viscous damping is not considered in our calculation of

resonance frequency. This is consistent with other systems in the literature where viscous effects are neglected when studying sessile drops [37, 46].

For a forced vibration without damping, the resonance frequency of a drop equals its natural frequency, which is proportional to $\sqrt{\gamma/m}$ or $\sqrt{\gamma/\rho R^3}$ [47-49]. Therefore, we set the characteristic frequency $\omega^* = \sqrt{\gamma/\rho R^3}$ in analogy to [44], eq. (1). During harmonic oscillation, the drop deformation is proportional to the drop size and vibration amplitude of the substrate. Thus, we use the drop radius R to non-dimensionalize the amplitude of substrate vibration Z. The corresponding characteristic amplitude of acceleration is then set as $a^* = R\omega^{*2}$. The values of non-dimensionalization factors with their respective drop properties are summarized in Table 1. Detailed information about how the liquid properties are obtained, especially for 50% v/v glycerol, is given in Appendix A. Matlab is used for the entire non-dimensionalization process (Appendix B).

Table 1. Summary of drop properties at 20 °C and calculated non-dimensionalization factors (see detail information in Appendix A).

	Unit	Water			50% v/v Glycerol
ρ	[kg/L]	0.998			1.147
γ	[mN/m]	71.68			68.25
μ	[mPa · s]	1.0			8.4
V	[μL]	5	8	13	8
$R = \sqrt[3]{3V/4\pi}$	[mm]	1.1	1.2	1.5	1.2
$Ca = \sqrt{\gamma/\rho g}$	[mm]	2.7			2.5
$Re = \sqrt{\rho\gamma R}/\mu$	/	275	298	323	37.1
$\omega^* = \sqrt{\gamma/\rho R^3}$	$[\frac{\text{rad}}{\text{s}}]$	245	194	152	177
$a^* = R\omega^{*2}$	$[\frac{\text{m}}{\text{s}^2}]$	63.8	46.7	33.8	38.7

3.2 Results

With the non-dimensionalization factors determined for each drop, we can non-dimensionalize the input frequency and the threshold amplitude of vibration by dividing ω with ω^* and a with a^*. The original data and the non-dimensionalized values for all four drops are given in Table 2 and Table 3, respectively.

Table 2. Original data for input frequencies and threshold acceleration of the texture ratchet.

Water						Glycerol	
5μL		8μL		13μL		8μL	
f [Hz]	a [g]	f [Hz]	a [g]	f [Hz]	a [g]	f [Hz]	a [g]
65	3.8	40	4.8	25	3.5	20	5.7
70	3	45	2.9	35	2.4	25	6.4
72.5	2.7	50	2.8	40	2.25	30	6.4
75	2.5	55	2.55	45	1.1	35	6
77.5	2.45	60	1.5	50	1.4	40	4.2
80	4.1	65	2.8	55	4.3	45	4
85	6.1	70	5.9	60	7.5	50	2.7
90	9.8					55	2.7
						60	4.0
						65	8.3
Note: The relationship between frequency f and angular frequency ω is $f = \omega/2\pi$.							

Table 3. Non-dimensionalized angular frequency and threshold acceleration.

Water						Glycerol	
5μL		8μL		13μL		8μL	
ω/ω^*	a/a^*	ω/ω^*	a/a^*	ω/ω^*	a/a^*	ω/ω^*	a/a^*
1.6649	0.0595	1.296	0.1029	1.0326	0.1037	0.7119	0.1475
1.793	0.047	1.458	0.0622	1.4456	0.0711	0.8899	0.1656
1.8571	0.0423	1.62	0.06	1.6521	0.0667	1.0679	0.1656
1.9211	0.0392	1.782	0.0547	1.8586	0.0326	1.2459	0.1552
1.9851	0.0384	1.944	0.0321	2.0651	0.0415	1.4239	0.1087
2.0492	0.0642	2.106	0.06	2.2716	0.1274	1.6019	0.1035
2.1772	0.0956	2.268	0.1264	2.4781	0.2222	1.7798	0.0698
2.3053	0.1535					1.9578	0.0698
						2.1358	0.1035
						2.3138	0.2147

The relationship between the non-dimensionalized input frequency ω/ω^* and amplitude of threshold acceleration a/a^* is shown in Figure 7.

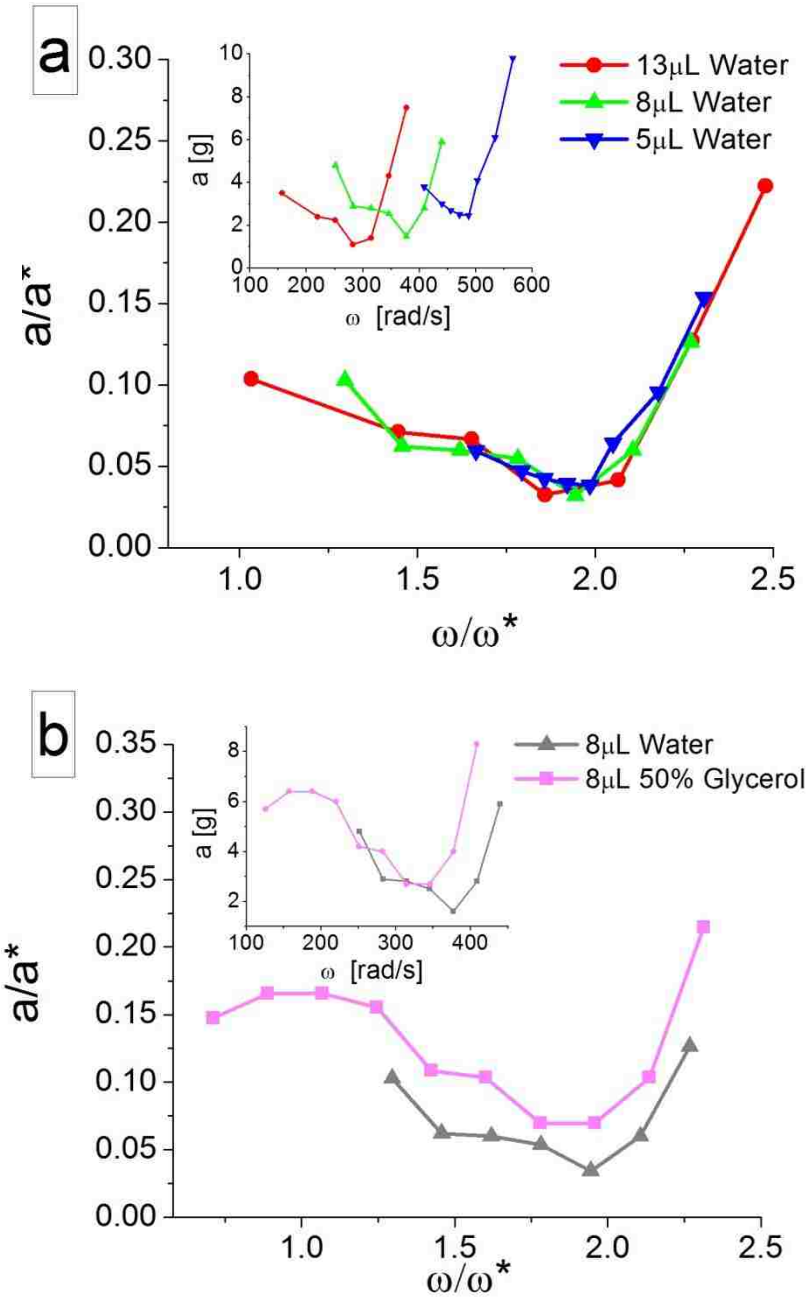

Figure 7. (a) Non-dimensionalized frequency versus amplitude of threshold acceleration for water drops with volumes of 5, 8, and 13 µL. (b) Non-dimensionalized frequency versus amplitude of threshold acceleration for 8 µL drops of water and 50% v/v glycerol. The insets correspond to the raw data shown in Figure 5.

For the three water drops with different volumes in Figure 7a, it is evident that the curves coincide with each other after non-dimensionalization, indicating that the behavior of water drops is consistent across drops with different volumes. The minimum acceleration corresponds to the resonance frequency of the drop, which requires the least amount of vibration to initiate motion. Figure 7b makes a comparison between a water drop and a 50% v/v glycerol drop with the same volume. The non-dimensionalized curves of both drops show a similar trend and there is a consistent match between them in terms of frequency. However, a difference in threshold amplitude remains even after non-dimensionalization, where a 50% v/v glycerol drop requires higher amplitude of vibration to initiate motion.

There may be several reasons for this discrepancy in amplitude. First, a 50% v/v glycerol drop beads up less than a pure water drop on a hydrophobic surface due to higher mass and lower surface tension (see Figure 8). The larger footprint of the glycerol drop pins it more strongly to the substrate, which in return requires a higher acceleration to release the drop and initiate motion. Second, as the glycerol drop is not as spherical as a water drop, R may no longer scale linearly with amplitude when calculating a^*. Finally, a/a^* represents normalized acceleration of the substrate; since higher viscosities lead to smaller drop deformations at resonance, glycerol drops will require higher threshold amplitudes.

These arguments can be extended further. According to Lamb [47] the resonance mode frequency for a drop in mode n is $f_r = \sqrt{n(n-1)(n+2)\frac{\gamma}{3\pi\rho V}}$, which with $n = 2$ yields

$\omega_r = \sqrt{8}\omega^*$. One would thus expect to see the minimum threshold acceleration near $\omega/\omega^* \approx 2.8$, but the observed value is somewhat lower (see again 7a and b). Furthermore, the quality factor, which indicates the amplification of an input signal at resonance is given by $Q = \omega_0 \frac{m}{b}$ with resonance frequency ω_0, mass m and damping coefficient b. Therefore, for the 8 µL water and glycerol drops, we would expect approximately an 8.4:1 ratio in the respective quality factors. We attribute these discrepancies to the fact that neither water nor glycerol form perfectly spherical drops on the texture ratchet, and to the complex pin-release behavior along the solid-liquid-air contact line during ratcheting motion.

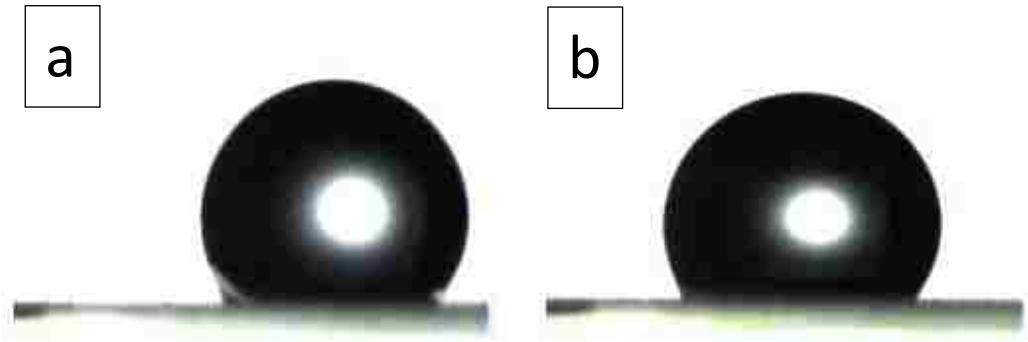

Figure 8. (a) Side view of an 8µL water drop sitting on the texture ratchet. (b) Side view of an 8µL 50% v/v glycerol drop.

3.3 Discussion of an alternative non-dimensionalization method

In the previous analysis, we can see that our non-dimensionalization method shows good results for water drops with different volumes. However for the two drops with same volume but all different other properties, the non-dimensionalization works for frequency, but not for threshold amplitude of vibration. A reasonable explanation for

this discrepancy was presented, indicating that the shape of the drop on the hydrophobic surface may play a role.

When studying the vibration of a sessile drop, Celestini and Kofman [50] took into account the surface area and the volume of a truncated sphere, and introduced a method to perform non-dimensionalization, with the non-dimensionalization factor for frequency given below.

$$\omega^{**} = \sqrt{\frac{6\gamma h(\theta)}{\rho(1-\cos\theta)(2+\cos\theta)}} R'^{-3/2}$$

As shown in Figure 9, θ is the contact angle of the sessile drop and R' is relative radius, which is defined as the distance from the center of the drop to the farthest edge. $h(\theta)$ is a geometry dependent factor and is described as a function of θ as shown in [50]. These three factors together describe the shape of the drop on a hydrophobic surface.

The non-dimensionalization factor for acceleration is then

$$a^{**} = V^{1/3}\omega^{**2}$$

where $V^{1/3}$ is used here in replacement of R because they are linearly related.

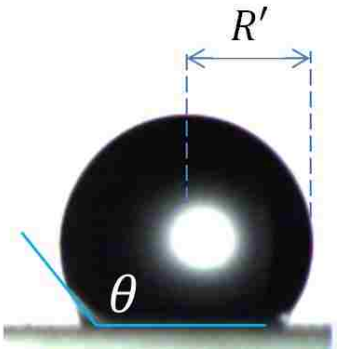

Figure 9. Contact angle $\boldsymbol{\theta}$ and relative radius $\boldsymbol{R'}$ of a sessile drop on a hydrophobic surface.

After a rough analysis of the two drops in Figure 8, an estimate of the contact angle θ, the corresponding $h(\theta)$ and R' is shown in Table 4. Note that R' is a numerical value with unit in pixel instead of the real length. However, this will not affect the non-dimensionalization result as pixel is linearly related to length. Therefore, from equation x, we can calculate the two non-dimensionalization factors ω^{**} and a^{**}.

Table 4. Characteristics of 8μL water and drops and an 8μL 50% v/v glycerol drop.

	Water	50% v/v Glycerol
θ [degree]	140	120
$h(\theta)$	0.150	0.325
R' (pixels)	82	88
ω^{**}	1.016×10^{-5}	1.200×10^{-5}
a^{**}	2.0635×10^{-13}	2.8817×10^{-13}

Accordingly, the result of non-dimensionalized frequency and amplitude of vibration is given in the following Table 5 and Figure 10.

Table 5. Non-dimensionalized angular frequency and threshold acceleration for the comparison between an 8µL water and drops and an 8µL 50% v/v glycerol drop.

Water (8µL)		Glycerol (8µL)	
ω/ω^{**} ($\times 10^7$)	a/a^{**} ($\times 10^{13}$)	ω/ω^{**} ($\times 10^7$)	a/a^{**} ($\times 10^{13}$)
3.4265	7.1913	1.4446	6.0711
3.8549	4.3447	1.8057	6.8166
4.2832	4.1949	2.1669	6.8166
4.7115	3.7455	2.528	6.3906
5.1398	2.3971	2.8891	4.4734
5.5681	4.1949	3.2503	4.2604
5.9965	8.8393	3.6114	2.8758
		3.9726	2.8758
		4.3337	4.2604
		4.6948	8.8403

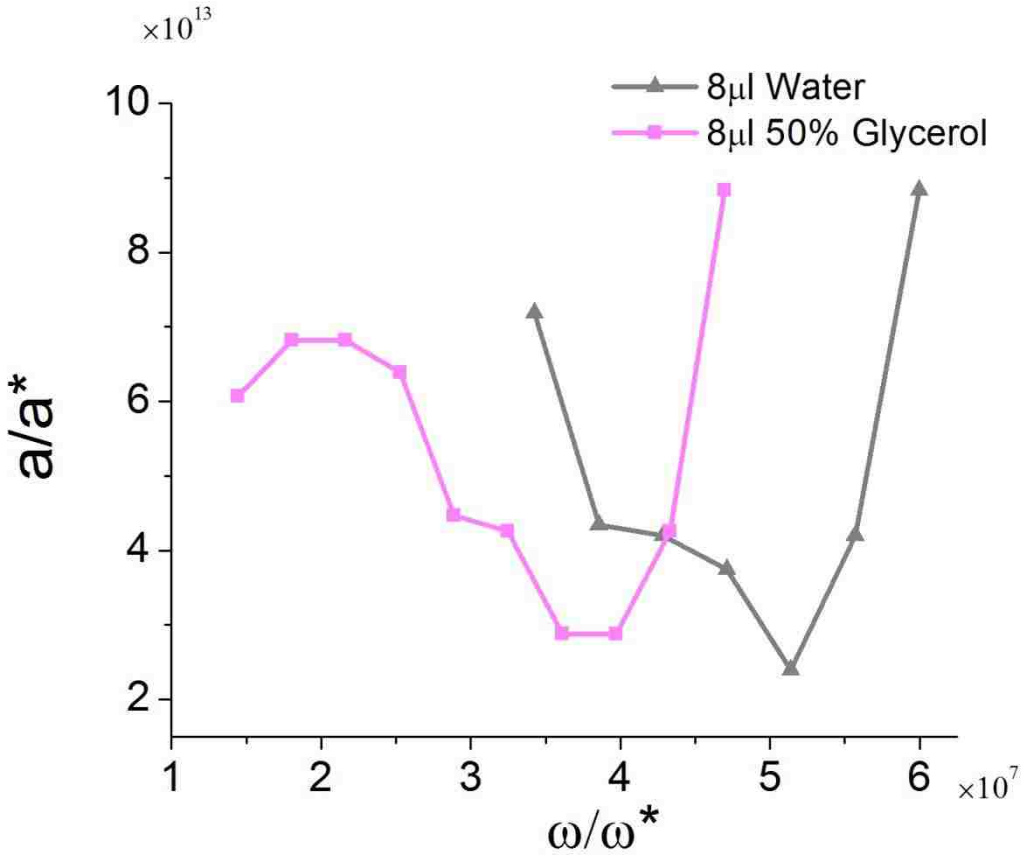

Figure 10. Non-dimensionalization result by Celestini's method. Non-dimensionalized frequency versus amplitude of threshold acceleration for 8 µL drops of water and 50% v/v glycerol.

Figure 10 shows that after Celestini and Kofman's non-dimensionalization process, there is a good match between the two drops in terms of amplitude of vibration. However, the offset in frequency still remains. This result may give some hints for a better non-dimensionalization method in the future.

In conclusion, our method introduced in the beginning of this chapter is satisfactory as it gives a good result for the water drop, which is the major object in most sessile drop studies. A general relationship between the input frequency and threshold amplitude of vibration is found, which can be used to predict the minimum amplitude of vibration needed to initiate drop motion at a certain frequency.

Chapter 4

Modeling Horizontal Drop Motion Driven by Vertical Vibration of Texture Ratchet

As the previous section has shown, the relationship between dimensionless frequency and amplitude of threshold acceleration suggests that the drop motion on a vibrating texture ratchet is a general phenomenon that occurs consistently across drops with different properties. However, it is still unclear how vertical vibration translates into horizontal drop motion. Nevertheless, a few theoretical and experimental studies have made significant advances in understanding the drop motion under horizontal or combined horizontal-vertical vibrations [37-41, 51]. These studies generally consider the forces acting on the drop at its center of mass and at its contact line, i.e., along the footprint defined by the solid-liquid-air interface. It is understood that vibrations cause non-equilibrium pin-release forces along the contact line. Surface tension couples the center of mass to the contact line. Therefore, during each oscillation cycle, the center of mass proceeds in response to this non-equilibrium force. On texture ratchets, the asymmetric forces between the leading and trailing edge of the drop arise from the directional curved rungs across which the drop is moving. In order to better understand this phenomenon, we hereby propose a compact model that captures the essential features of this system and that qualitatively explains how a pure vertical vibration can translate into a horizontal drop motion. Since there is no net drop motion in the

transverse direction, our model will focus on the drop behavior in the cross-sectional plane centered along the ratchet track.

4.1 Drops on texture ratchets as mass-spring-damper systems

Recall that for non-dimensionalization, viscous damping was neglected while determining the resonance frequency of the drop; this simplification is adequate when describing the behavior of the drop before lateral motion occurs. However, damping effects need to be taken into account when the drop is moving along the track as they cause friction or drag, both inside the drop and at its interface with the ratchet track. Damping also determines how much energy is coupled into the drop from the oscillating platform and how quickly it is dissipated. Periodic external forces due to vibration act on the drop at its leading and trailing edge; in our cross-sectional model, these edges are represented as points Q and P, which are connected to the center of mass R and to each other by damped springs. Figure 11a illustrates this drop model as a triangular mass-spring-damper system. The mass at the center m_{R} corresponds to the bulk volume of the drop, while the two masses at the leading and trailing edges (respectively, m_{Q} and m_{P}) correspond to the drop regions along the contact line; accordingly, we assume that the edge masses are equal and both smaller than the center mass ($m_{\mathrm{P}} = m_{\mathrm{Q}} < m_{\mathrm{R}}$). The springs between P, Q and R represent surface tension; we assume $k_{\mathrm{PR}} = k_{\mathrm{QR}} < k_{\mathrm{PQ}}$ because pin-release events at the contact line create the effect of a stiffer spring. For simplicity, we assume that the lengths of the springs under zero load are equal

($l_{PR} = l_{QR} = l_{PQ}$), and that the viscous damping coefficient b is the same for all dampers and given by Stokes' law as $b = 6\pi\mu R$.

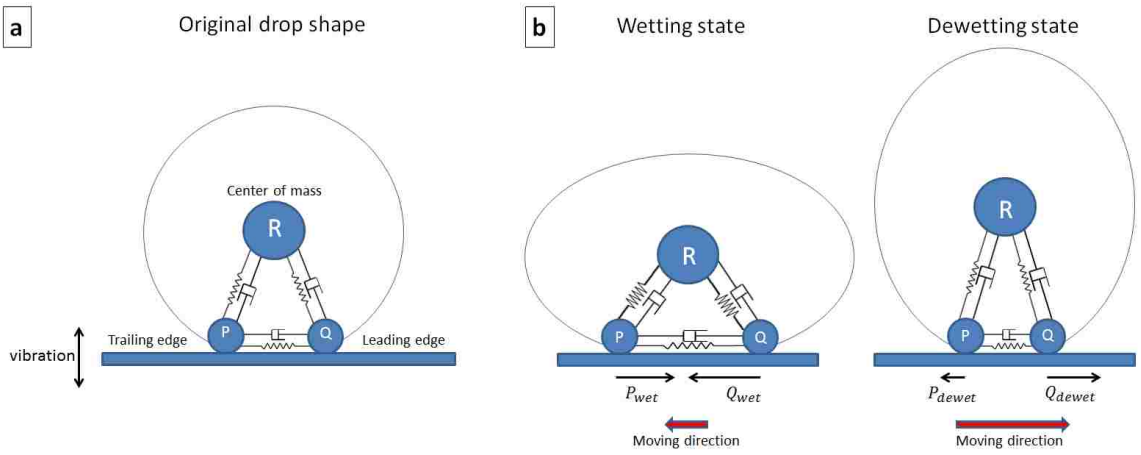

Figure 11. (a) Sessile drop in equilibrium modeled with a triangular mass-spring-damper system. (b) The deformation and motion of a drop during one cycle of vertical vibration. The drop flattens and moves backwards (left) during wetting, and beads up and moves forward (right) during dewetting. The pin-release forces are modeled as friction forces at the leading and trailing edges.

4.2 Force asymmetry along the contact line

During each vibration cycle, the drop undergoes advancing (wetting) and receding (dewetting) motion with time-varying pin-release forces acting at the contact line of the drop (Figure 11b). In general, these pin-release forces have components in the x, y and z directions. However, since the texture ratchet is symmetric with respect to the central axis of the track (see Figure 2 and 3), the net force in the transverse direction (y-axis) must be zero. Furthermore, as we are primarily interested in the lateral motion of the drop, let us consider only the horizontal portion of the pin-release forces. These forces are opposite in direction to the local motion of the contact line, and can therefore be interpreted as friction. We aggregate all pin-release forces at the footprint of the drop

into two combined forces at the leading and trailing edges, F_Q and F_P, respectively. The relationship between F_Q and F_P is the key to understanding how the texture ratchet works: if we can show that the sum of F_Q and F_P, integrated over one period of oscillation, is non-zero, then we can expect lateral drop motion.

To complete this argument, we make several observations. First, because of the geometric design of the rungs, the solid-liquid portion of the contact line is larger at the leading edge. In other words, the drop footprint is conforming to the curvature of the rung along the leading edge while bridging several gaps between rungs along the trailing edge. Therefore, F_Q is always larger in magnitude than F_P, or more specifically $|F_{Q,wet} > F_{P,wet}|$ and $|F_{Q,dewet} > F_{P,dewet}|$, and thus the drop experiences a net backward motion during wetting and a net forward motion during dewetting. It remains to be shown that these two motions do not cancel out over a complete cycle of vibration.

The second observation was obtained by Shastry and co-workers [32, 34], who noted that the receding contact angles of the two edges differ more than the advancing contact angles; typically, this will lead to $|F_{Q,dewet} - F_{P,dewet}| > |F_{Q,wet} - F_{P,wet}|$, which suggests that forward motion during dewetting is larger than backward motion during wetting. Finally, since the advancing contact angle on a textured hydrophobic surface is close to 180° while the receding contact angle is closer to 90°, it follows that $|F_{Q,wet}| > |F_{Q,dewet}|$ and $|F_{P,wet}| > |F_{P,dewet}|$. It is consistent with a related observation by Dorrer and Rühe [52] stating that wetting in general is less sensitive to texture than

dewetting. In combination, these observations indicate that lateral drop motion in the direction of the rung curvature (positive x-direction in Figure 3) can be expected once the vibration reaches the threshold for contact line motion.

4.3 Simulation of drop motion

We have created a simulation for drop motion that models the drop as a two-dimensional triangular mass-spring-damper system with friction forces as described above. As we are studying the drop motion, the displacement of the three masses in both x and z axes are set to be our independent variables. For each mass in each direction, the total force including inertia, spring force, damping force, normal force and friction, needs to be zero. Therefore, a total set of six equations can be set up to solve this problem with six degrees of freedom.

Regarding initial and boundary conditions, we start the simulation in an equilibrium state of the drop. During simulation, the two edge points P and Q are assumed to always remain in contact with the substrate. Since the substrate vibrates vertically with a sinusoidal signal at frequency ω and amplitude Z, the displacement of the edge masses m_{P} and m_{Q} is always $z(t) = Z\sin(\omega t)$. This effectively reduces the system to 4 degrees of freedom with 4 unknowns.

In conventional dry friction models, the friction force is the product of friction coefficient, magnitude of normal force and negated unit velocity vector. Such models often cause difficulties in simulations since the time-varying normal force is unknown a priori, resulting in a system that cannot be described by second-order ordinary

differential equations. However, in our case viscosity and pin-release action are the dominant sources of friction, which are both independent of normal force. Viscous forces are linear in mass, velocity and viscosity, while pin-release forces are simple step functions that we approximate with smooth sigmoid functions, leading to a system of differential equations that can be simulated numerically with standard techniques.

A detailed explanation of how the model is set up can be found in Appendix C. Simulation process using Mathematica is given in Appendix D.

4.4 Modeling: results and discussion

Figure 12 shows the result of drop position in the horizontal plane as a function of time. The three solid curves represent the location of the three masses m_{P}, m_{Q} and m_{R}, respectively. The amplitude of oscillation at the trailing edge (red) is always larger than at the leading edge (blue), which corresponds to the smaller friction at the trailing edge. Meanwhile, it can be observed that the leading and trailing edges usually move in opposite directions, but not always, and not always at the same rate; lateral motion is a consequence of this asymmetry. The experimental data adopted from Figure 6 is shown in the inset figure. There is good agreement between the model and the experimental data, indicating that our model and all associated parameters that are chosen provide a reasonable representation of the drop characteristics and behavior of drop motion. A series of pictures regarding the animation of the modeled drop motion can be found in the Appendix C.

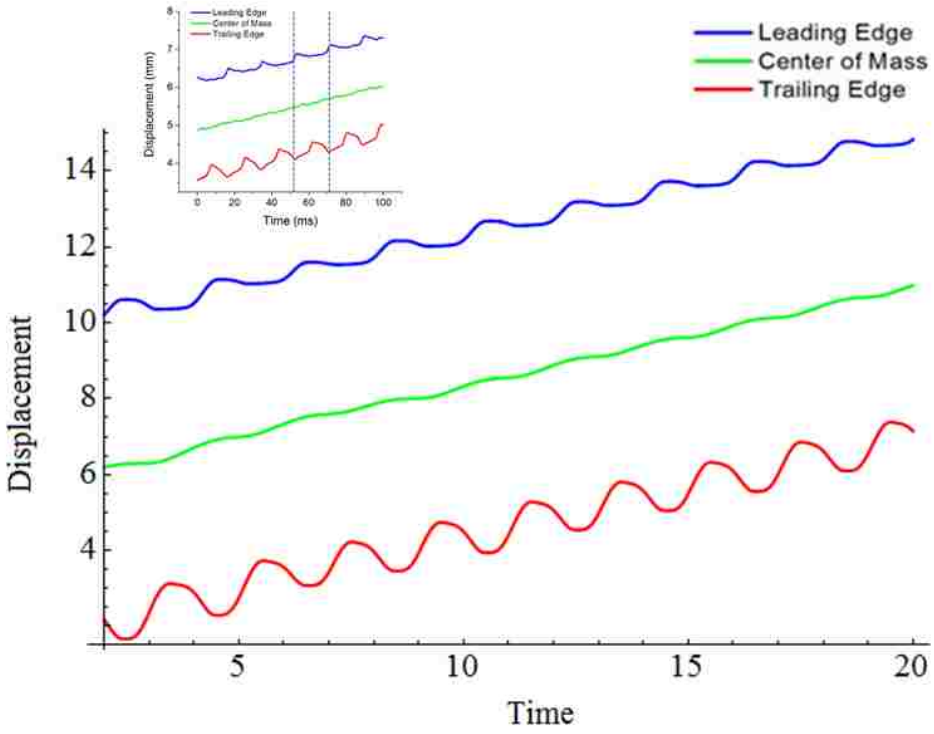

Figure 12. Lateral displacement of the drop at its center of mass (green), leading (blue) and trailing (red) edges. The model curves have less sharp corners when compared to the experimental data, because the friction is modeled with a continuous function to eliminate numerical instability during simulations.

In this system, there are two conditions that are not essential for our model: horizontal substrate and sinusoidal input signal. With modest adjustment, our model can be adapted to other systems such as inclined surfaces and sawtooth or square wave input. For inclined surfaces with a small tilted angle, an extra resistance force due to gravity will apply. However, the drop can still move uphill as long as the net uphill force dominates in each oscillation cycle. Yet for each drop, there is a critical angle beyond which no uphill motion can be observed. For other input signals such as a square wave function, net drop motion has been observed experimentally on a texture ratchet [32, 34]. In our model, the sinusoidal wave function can be easily replaced with a square

wave function. For a sinusoidal wave input, unexpected “overtones” of the base oscillation were observed by Fourier analysis [29], probably because of the stick-slip behavior of the contact line. With a square wave input, we would expect more such overtones, making the displacement curves more jagged.

Chapter 5

Conclusions and Future Work

This thesis presents a theoretical study of the horizontal drop motion on a vertically vibrating texture ratchet. By non-dimensionalizing the input frequency and threshold amplitude of vibration to initiate drop motion, we reveal a general relationship between these two input factors across drops with different characteristics. This relationship indicates that the condition to initiate drop motion on such a texture ratchet is predicable. Further study proposes an adequately complete model to describe, for the first time, how a lateral drop motion occurs under a vibration perpendicular to the substrate. The qualitative analysis reveals that the pin-release forces at the contact line are the driving force. With a surface with asymmetric features, the pin-release forces during vibration are also asymmetric between the leading and trailing edges of the drop, which results in a net drop motion in the lateral direction. The simulation results show good agreement with experimental data.

A final piece that is needed for this model is a detailed quantitative analysis of the effect of the contact line as it moves over the asymmetric textured surface. This may give further insights into the mechanism of such drop motion at the microscopic level.

Last but not least, we hypothesize that as the feature size of the texture ratchet shrinks, so does the energy required to move the liquid drops. The reasoning in support of this hypothesis is that the energy barrier that needs to be overcome (also known as the

contact angle hysteresis) is strongly related to feature size. Therefore, a nanoscale texture ratchet is being developed using electron beam lithography (Figure 13) in order to move liquid drops with minimal energy input. This design could lead to a generic platform for a low-cost compact diagnostic tool that could possibly be operated with a smartphone.

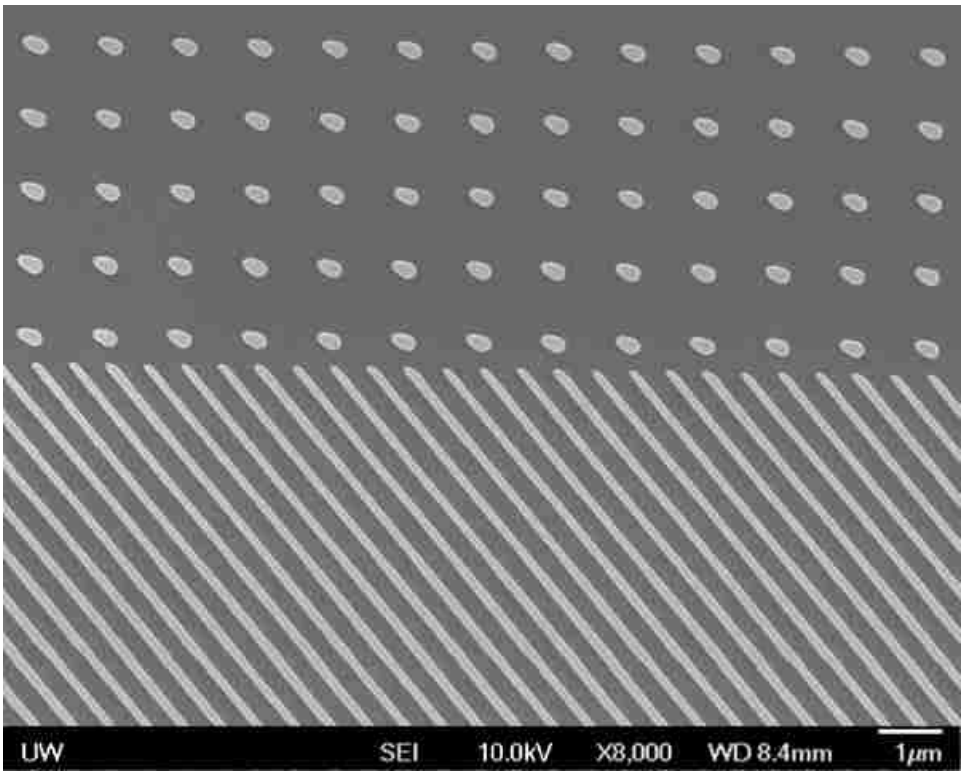

Figure 13. Nanoscale texture ratchet fabricated by electron beam lithography. The height of both the rungs (~100 nm in width) and the dots (~300 nm in diameter) is ~550 nm (SEM micrograph by Rick Bojko).

Bibliography

1. Stone, H.A., A.D. Stroock, and A. Ajdari, *Engineering flows in small devices: Microfluidics toward a lab-on-a-chip.* Annual Review of Fluid Mechanics, 2004. **36**: p. 381-411.
2. Weibel, D.B., et al., *Torque-actuated valves for microfluidics.* Analytical Chemistry, 2005. **77**(15): p. 4726-4733.
3. Laser, D.J. and J.G. Santiago, *A review of micropumps.* Journal of Micromechanics and Microengineering, 2004. **14**(6): p. R35-R64.
4. Nguyen, N.T. and Z.G. Wu, *Micromixers - a review.* Journal of Micromechanics and Microengineering, 2005. **15**(2): p. R1-R16.
5. Paegel, B.M., R.G. Blazej, and R.A. Mathies, *Microfluidic devices for DNA sequencing: sample preparation and electrophoretic analysis.* Current Opinion in Biotechnology, 2003. **14**(1): p. 42-50.
6. Liu, J., M. Enzelberger, and S. Quake, *A nanoliter rotary device for polymerase chain reaction.* Electrophoresis, 2002. **23**(10): p. 1531-1536.
7. Kleparnik, K. and M. Horky, *Detection of DNA fragmentation in a single apoptotic cardiomyocyte by electrophoresis on a microfluidic device.* Electrophoresis, 2003. **24**(21): p. 3778-3783.
8. Lee, G.B., et al., *Microfabricated plastic chips by hot embossing methods and their applications for DNA separation and detection.* Sensors and Actuators B-Chemical, 2001. **75**(1-2): p. 142-148.
9. Pihl, J., M. Karlsson, and D.T. Chiu, *Microfluidic technologies in drug discovery.* Drug Discovery Today, 2005. **10**(20): p. 1377-1383.
10. Dittrich, P.S. and A. Manz, *Lab-on-a-chip: microfluidics in drug discovery.* Nature Reviews Drug Discovery, 2006. **5**(3): p. 210-218.
11. Rasooly, A. and K.E. Herold, *Biosensors for the analysis of food- and waterborne pathogens and their toxins.* Journal of Aoac International, 2006. **89**(3): p. 873-883.

12. Meagher, R.J., et al., *An integrated microfluidic platform for sensitive and rapid detection of biological toxins.* Lab on a Chip, 2008. **8**(12): p. 2046-2053.
13. Teh, S.Y., et al., *Droplet microfluidics.* Lab on a Chip, 2008. **8**(2): p. 198-220.
14. Solvas, X.C.I. and A. deMello, *Droplet microfluidics: recent developments and future applications.* Chemical Communications, 2011. **47**(7): p. 1936-1942.
15. Joensson, H.N. and H. Andersson-Svahn, *Droplet microfluidics-a tool for protein engineering and analysis.* Lab on a Chip, 2011. **11**(24): p. 4144-4147.
16. Squires, T.M. and S.R. Quake, *Microfluidics: Fluid physics at the nanoliter scale.* Reviews of Modern Physics, 2005. **77**(3): p. 977-1026.
17. Atencia, J. and D.J. Beebe, *Controlled microfluidic interfaces.* Nature, 2005. **437**(7059): p. 648-655.
18. Brochard, F., *Motions of Droplets on Solid Surfaces Induced by Chemical or Thermal Gradients.* Langmuir, 1989. **5**: p. 432-438.
19. Chaudhury, M.K. and G.M. Whitesides, *How to Make Water Run Uphill.* Science, 1992. **256**(5063): p. 1539-1541.
20. Pollack, M.G., A.D. Shenderov, and R.B. Fair, *Electrowetting-based actuation of droplets for integrated microfluidics.* Lab on a Chip, 2002. **2**(2): p. 96-101.
21. Pollack, M.G., R.B. Fair, and A.D. Shenderov, *Electrowetting-based actuation of liquid droplets for microfluidic applications.* Applied Physics Letters, 2000. **77**(11): p. 1725-1726.
22. Cho, S.K., H.J. Moon, and C.J. Kim, *Creating, transporting, cutting, and merging liquid droplets by electrowetting-based actuation for digital microfluidic circuits.* Journal of Microelectromechanical Systems, 2003. **12**(1): p. 70-80.
23. Zhang, J.H., et al., *Ratchet-induced anisotropic behavior of superparamagnetic microdroplet.* Applied Physics Letters, 2009. **94**(14).
24. Linke, H., et al., *Self-propelled Leidenfrost droplets.* Physical Review Letters, 2006. **96**(15).
25. Lagubeau, G., et al., *Leidenfrost on a ratchet.* Nature Physics, 2011. **7**(5): p. 395-398.

26. Buguin, A., L. Talini, and P. Silberzan, *Ratchet-like topological structures for the control of microdrops.* Applied Physics a-Materials Science & Processing, 2002. **75**(2): p. 207-212.
27. Daniel, S., et al., *Ratcheting motion of liquid drops on gradient surfaces.* Langmuir, 2004. **20**(10): p. 4085-4092.
28. Buguin, A., F. Brochard, and P.G. de Gennes, *Motions induced by asymmetric vibrations - The solid/solid case.* European Physical Journal E, 2006. **19**(1): p. 31-36.
29. Duncombe, T.A., et al., *Controlling Liquid Drops with Texture Ratchets.* Advanced Materials, 2012. **24**(12): p. 1545-1550.
30. Prakash, M., D. Quere, and J.W.M. Bush, *Surface tension transport of prey by feeding shorebirds: The capillary ratchet.* Science, 2008. **320**(5878): p. 931-934.
31. Tilney, L.G. and D.A. Portnoy, *Actin-Filaments and the Growth, Movement, and Spread of the Intracellular Bacterial Parasite, Listeria-Monocytogenes.* Journal of Cell Biology, 1989. **109**(4): p. 1597-1608.
32. Shastry, A., M.J. Case, and K.F. Bohringer, *Directing droplets using microstructured surfaces.* Langmuir, 2006. **22**(14): p. 6161-6167.
33. Chaudhury, M.K., S. Sircar, and S. Daniel, *Rectified motion of liquid drops on gradient surfaces.* Abstracts of Papers of the American Chemical Society, 2003. **225**: p. U679-U679.
34. Shastry, A.T., D; Bohringer, K. F., *Micro-Structured Surface Ratchets for Droplet Transport.* Transducers and Eurosensors, 2007.
35. Duncombe, T.A., J.F. Parsons, and K.F. Bohringer, *Directed Drop Transport Rectified from Orthogonal Vibrations via a Flat Wetting Barrier Ratchet.* Langmuir, 2012. **28**(38): p. 13765-13770.
36. Quere, D., *Surface chemistry - Fakir droplets.* Nature Materials, 2002. **1**(1): p. 14-15.
37. Noblin, X., R. Kofman, and F. Celestini, *Ratchetlike Motion of a Shaken Drop.* Physical Review Letters, 2009. **102**(19).

38. Malvadkar, N.A., et al., *An engineered anisotropic nanofilm with unidirectional wetting properties.* Nature Materials, 2010. **9**(12): p. 1023-1028.
39. Daniel, S., M.K. Chaudhury, and P.G. de Gennes, *Vibration-actuated drop motion on surfaces for batch microfluidic processes.* Langmuir, 2005. **21**(9): p. 4240-4248.
40. Mettu, S. and M.K. Chaudhury, *Motion of drops on a surface induced by thermal gradient and vibration.* Langmuir, 2008. **24**(19): p. 10833-10837.
41. Mettu, S. and M.K. Chaudhury, *Motion of Liquid Drops on Surfaces Induced by Asymmetric Vibration: Role of Contact Angle Hysteresis.* Langmuir, 2011. **27**(16): p. 10327-10333.
42. Goohpattader, P.S., S. Mettu, and M.K. Chaudhury, *Stochastic rolling of a rigid sphere in weak adhesive contact with a soft substrate.* European Physical Journal E, 2011. **34**(11).
43. Goohpattader, P.S. and M.K. Chaudhury, *Random motion with interfacial contact: Driven diffusion vis-à-vis mechanical activation.* European Physical Journal E, 2012. **35**(67).
44. Vukasinovic, B., M.K. Smith, and A. Glezer, *Dynamics of a sessile drop in forced vibration.* Journal of Fluid Mechanics, 2007. **587**: p. 395-423.
45. Wilkes, E.D. and O.A. Basaran, *Forced oscillations of pendant (sessile) drops.* Physics of Fluids, 1997. **9**(6): p. 1512-1528.
46. Noblin, X., A. Buguin, and F. Brochard-Wyart, *Vibrated sessile drops: Transition between pinned and mobile contact line oscillations.* European Physical Journal E, 2004. **14**(4): p. 395-404.
47. Lamb, H., *Hydrodynamics*1932, Cambridge, U.K.: Cambridge University Press.
48. McHale, G., et al., *Levitation-Free Vibrated Droplets: Resonant Oscillations of Liquid Marbles.* Langmuir, 2009. **25**(1): p. 529-533.
49. Sharp, J.S., D.J. Farmer, and J. Kelly, *Contact Angle Dependence of the Resonant Frequency of Sessile Water Droplets.* Langmuir, 2011. **27**(15): p. 9367-9371.
50. Celestini, F. and R. Kofman, *Vibration of submillimeter-size supported droplets.* Physical Review E, 2006. **73**(4).

51. Goohpattader, P.S. and M.K. Chaudhury, *Random motion with interfacial contact: Driven diffusion vis-a-vis mechanical activation.* European Physical Journal E, 2012. **35**(8).
52. Dorrer, C. and J. Ruhe, *Some thoughts on superhydrophobic wetting.* Soft Matter, 2009. **5**(1): p. 51-61.
53. Cheng, N.S., *Formula for the viscosity of a glycerol-water mixture.* Industrial & Engineering Chemistry Research, 2008. **47**(9): p. 3285-3288.
54. *Physical properties of glycerine and its solutions.* Glycerine Producers Association, 1963.

Appendix A

The liquid properties of water can be found from various literatures. Therefore, only the method to obtain the liquid properties of 50% v/v glycerol-water mixture is stated here.

Density and viscosity

Cheng et al. performed a complete study and proposed an empirical formula for the calculation of the viscosity of glycerol-water mixture for mass concentration in the range of 0-100% and temperatures varying from 0 to 100^{o}C [53]. A useful tool based on their study is created on the following website for quick calculation of the density and viscosity of glycerol-water mixtures with different volume ratio.

< http://www.met.reading.ac.uk/~sws04cdw/viscosity_calc.html>

In our case for a 50% v/v mixture, the volume of both components is set to be 1 L, and the result is shown as below. Density is 1.147kg/L and viscosity is 8.4 mPa·s.

Calculate density and viscosity of glycerol/water mixtures

Enter temperature [C]: 20

Enter volume of water [litres]: 1

Enter volume of glycerol [litres]: 1

Click this button to do the sum: Calculate

Fraction of glycerol by volume is: 0.50000

Fraction of glycerol by mass is: 0.55878

Density of mixture is [kg/m^3]: 1146.6

Dynamic viscosity of mixture is [Ns/m^2]: 0.0083968

Kinematic viscosity of mixture is [m^2/s]: 0.0000073232

Based on the parameterisation in Cheng (2008) *Ind. Eng. Chem. Res.* **47** 3285-3288

Surface tension

Previous literatures have studied the properties of water-glycerol mixture against the percentage of glycerol by weight [54]. From there we obtain surface tension with glycerol % by weight at 20°C.

Table 6. Surface tension of glycerol with different % by weight at 20°C.

Glycerol % by weight	99.19	81.98	61.44	39.31	20.29	0.0
Surface tension of Glycerol [mN/m]	—	65.26	67.64	—	70.93	71.68

The four data points are plotted to show the relationship between glycerol mixture % by weight and surface tension. A quadratic function is then used to fit the curve. Known from the previous calculation, the fraction of glycerol by weight is about 55% if the volume ratio is 1:1. We can then see from Figure 13 that the surface tension of 50% v/v glycerol is 68.25 mN/m.

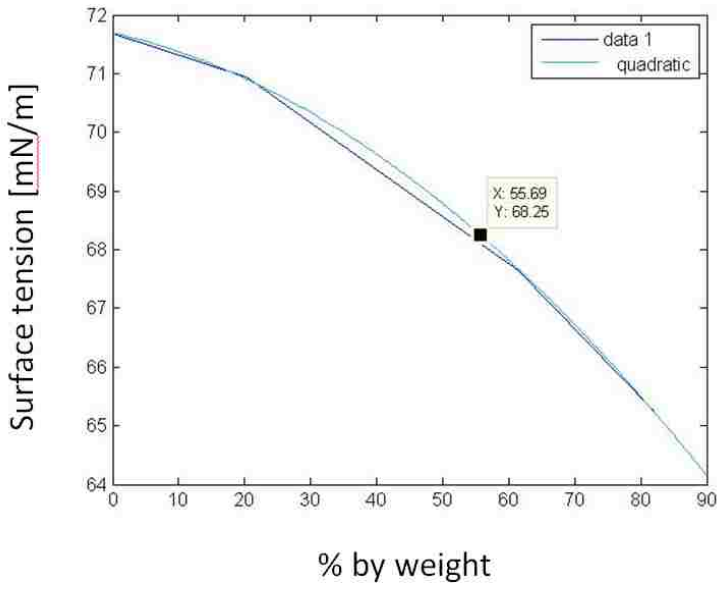

Appendix B

Matlab code for non-dimensionalization with detailed drop properties

```
% Fig. 3a original data from Yegan Erdem

volume5 = 5*10^-9; %[m^3]
volume8 = 8*10^-9; %[m^3]
volume13 = 13*10^-9; %[m^3]

R5 = (3*volume5/4/pi)^(1/3);
R8 = (3*volume8/4/pi)^(1/3);
R13 = (3*volume13/4/pi)^(1/3);

etaWater = 0.001005; % [Pa s][m]=[N/m^2 s][m]=[N/m s] % Viscosity at 20 C: water 1.005 mPa s, glycerol
1.2 Pa s
etaGlycerol = 0.0084; % 50% v/v = 55.9% wt Glycerol aqueous solution [Physical properties of Glycerine
and its solutions]

gammaWater = 71.68*10^-3;  %[N/m] % Surface tension: water 71.97 mN/m at 25 C, glycerol 63 mN/m at
20 C
gammaGlycerol = 68.25*10^-3; % 50% Glycerol aqueous solution [Physical properties of Glycerine and its
solutions]

rhoWater = 0.998*10^3; %[kg/m^3]
rhoGlycerol = 1.147*10^3; % 50% Glycerol aqueous solution [Physical properties of Glycerine and its
solutions]

%%%%%%%%%%%%%%%%%%%
Re_W_5 = sqrt(rhoWater*gammaWater*R5)/etaWater;
%274
Re_W_8 = sqrt(rhoWater*gammaWater*R8)/etaWater;

Re_W_13 = sqrt(rhoWater*gammaWater*R13)/etaWater;

Re_G = sqrt(rhoGlycerol*gammaGlycerol*R8)/etaGlycerol;
%37

%%%%%%%%%%%%%%%%%%%%%%%%%%%%%%%%%%%%%%%%%%%%%%%%%%%%%%%%%%%%%%%%%%%
%%%%%%%%%%%%
% Water with different volumes

% Original data of the input [frequency/Hertz acceleration/gravity]
drop5 = [65 3.8; 70 3; 72.5 2.7; 75 2.5; 77.5 2.45; 80 4.1; 85 6.1; 90 9.8];
drop8 = [40 4.8; 45 2.9; 50 2.8; 55 2.55; 60 1.5; 65 2.8; 70 5.9];
drop13 = [25 3.5; 35 2.4; 40 2.25; 45 1.1; 50 1.4; 55 4.3; 60 7.5];
```

```
figure(1); clf;
plot(2*pi*drop13(:,1),drop13(:,2),'r-o',2*pi*drop8(:,1),drop8(:,2),'b-o',2*pi*drop5(:,1),drop5(:,2),'g-o');
xlabel('Frequency [Hz]');
ylabel('Acceleration [g]');


%non-dimensionalization factors f0 = 1/2 pi *sqrt(k/m) & a0 = (2 pi f0)^2*V^(1/3)
w0_13 = sqrt(gammaWater/(R13^3*rhoWater));
w0_8 = sqrt(gammaWater/(R8^3*rhoWater));
w0_5 = sqrt(gammaWater/(R5^3*rhoWater));

a0_13 = R13*w0_13^2;
a0_8 = R8*w0_8^2;
a0_5 = R5*w0_5^2;

%dimensionless f and a
drop13w = 2*pi*drop13(:,1)/w0_13;
drop8w = 2*pi*drop8(:,1)/w0_8;
drop5w = 2*pi*drop5(:,1)/w0_5;

drop13a = drop13(:,2)/a0_13;
drop8a = drop8(:,2)/a0_8;
drop5a = drop5(:,2)/a0_5;

figure(2);clf;
plot(drop13w,drop13a,'r-o',drop8w,drop8a,'b-o',drop5w,drop5a,'g-o');
xlabel('w/w_0');
ylabel('a/a_0');


%%%%%%%%%%%%%%%%%%%%%%%%%%%%%%%%%%%%%%%%%%%%%%%%%%%%%%%%%%%%%%%%%%%
%%%%%%%%%%%%%
% Water&Glycerol
dropWater    = [40 4.8; 45 2.9; 50 2.8; 55 2.5; 60 1.6; 65 2.8; 70 5.9];
dropGlycerol = [20 5.7; 25 6.4; 30 6.4; 35 6; 40 4.2; 45 4; 50 2.7; 55 2.7; 60 4; 65 8.3];

figure(3); clf;
plot(2*pi*dropWater(:,1),dropWater(:,2),'b-o',2*pi*dropGlycerol(:,1),dropGlycerol(:,2),'k-o');
xlabel('frequency  [Hz]');
ylabel('acceleration  [g]');

%non-dimensionalization factors f0 = 1/2 pi *sqrt(k/m) & a0 = (2 pi f0)^2*V^(1/3)
w0_G = sqrt(gammaGlycerol/(R8^3*rhoGlycerol));
w0_W = sqrt(gammaWater/(R8^3*rhoWater));

a0_G = R8*w0_G^2;
a0_W = R8*w0_W^2;

dropWaterw = 2*pi*dropWater(:,1)/w0_W;
```

```
dropGlycerolw = 2*pi*dropGlycerol(:,1)/w0_G;

dropWatera = dropWater(:,2)/a0_W;
dropGlycerola = dropGlycerol(:,2)/a0_G;

figure(4); clf;
plot(dropWaterw,dropWatera,'b-o',dropGlycerolw,dropGlycerola,'k-o');
xlabel('w/w_0');
ylabel('a/a_0');

%%%%%%%%%%%%%%%%%%%%%%%%%%%%%%%%%%%%%%%%%%%%%%%%%%%%%%%%%%%%%%
%%%%%%%%%%%%
```

Appendix C

Mathematical modeling

To study the drop motion in the triangle mass-spring-damper system, there are six independent variables, x_p, z_p, x_q, z_q, x_R, z_R, which correspond to the displacement of each mass in both x and y directions (Figure 13). A set of six force balance equations is therefore needed to solve these six degrees of freedom.

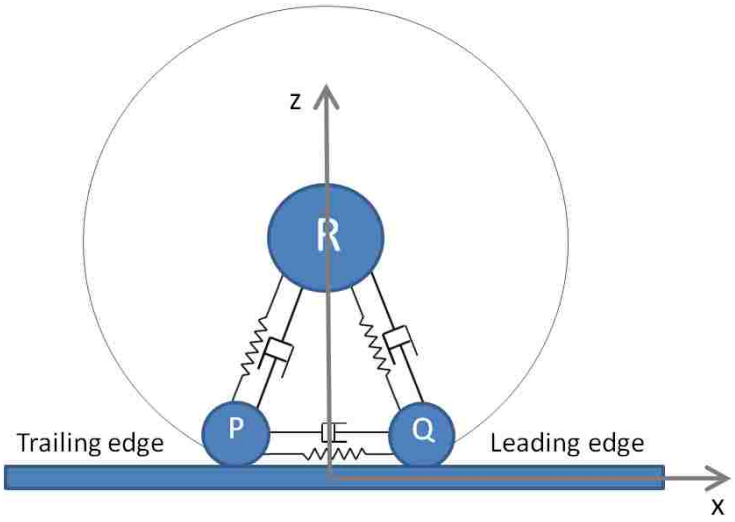

Figure 14. x-z coordinate for a triangle mass-spring-damper system.

Each force balance equation includes inertia, spring force, damping force, normal force and friction (pin-release force). For each mass at either direction, the total force must be zero. A general equation is given below.

$$\sum F_{ij} = 0 \qquad (i = P, Q, R \quad j = x, z)$$

Inertia is the product of mass and acceleration. Spring force is the product of spring constant and change in spring length. Damping force is the product of damping

coefficient and relative speed. Although the time-varying normal force and friction are unknown a priori, for reasons stated in Chapter 4, we set normal force to be gravity and define an auxiliary function here for the anisotropic dynamic friction coefficient with

$$\mu_k = \begin{cases} \mu_{k-} & v < 0 \\ 0 & v = 0 \\ -\mu_{k+} & v > 0 \end{cases} \qquad (k = P, Q)$$

where v is the velocity of the drop edge relative to the supporting substrate. μ_{k-} and μ_{k+} are non-negative, causing the friction (if existent) to be opposed to the direction of motion. However, in practical simulations, a non-continuous definition of the friction coefficient may cause numerical instabilities; therefore a smooth approximation (in analogy to the definition of the hyperbolic tangent "tanh") is used:

$$\mu_k = \frac{e^{sv} - e^{-sv}}{\frac{e^{sv}}{-\mu_{k+}} - \frac{e^{-sv}}{\mu_{k-}}}$$

where s is a scaling factor that determines the sharpness of the step at $v = 0$, with larger s causing a sharper step. Detailed modeling with assigned parameters is coded with Mathematica and is shown in Appendix D.

Simulation result

The simulation of the triangle mass-spring-damper model is shown in the following time series figures. Initially, the drop is in this steady state without any movement. When under vibration, the leading and trailing edges moves up and down in the vertical direction together with the substrate, and advance or recede in the horizontal plane. Because of the pin-release asymmetry, a net forward motion is observed in each oscillation cycle.

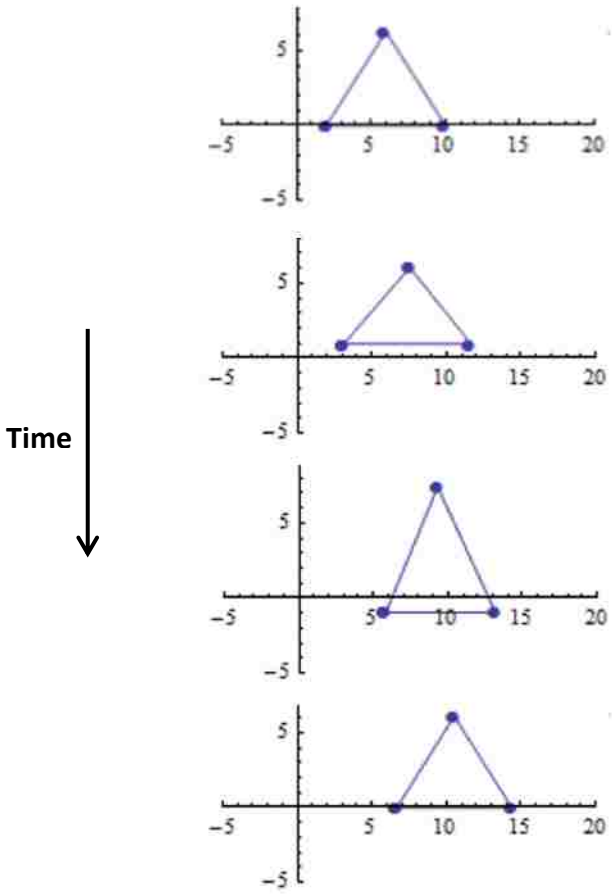

Figure 15. Time series pictures of the simulation of drop motion. Note that the four pictures are taken from different oscillation cycles to exaggerate the phenomenon.

Appendix D

Mathematica modeling

Karl F. Böhringer / Yan Dong, 31 December 2011 - 10 December 2012

This document describes a model of a sessile drop as it responds to agitation of the substrate surface on which it is sitting. The surface or the agitation may be anisotropic, such that a "ratcheting" motion of the drop can be observed.

Basic Setup and Tools

Model Setup

This is a two-dimensional model that looks at the vertical cross-section of a drop through its center of mass. The substrate coincides with the x-axis when it is at rest (not moving).

- **Physical Parameters**
- **Gravity**

Gravity usually points in the -y direction, but this can be changed to model inclined surfaces.

```
Gx = 0; Gy = -1; G = {Gx, Gy};
```

- **Friction**

Friction is modeled here as general anisotropic dry friction, which always opposes motion. We define here an auxiliary function for the anisotropic dynamic friction coefficient with mu(v,fl,fr) such that mu = fl if v<0, mu = 0 if v=0, and mu=-fr if v>0. The friction is then given by multiplying mu with the normal force. In practice, a non-continuous definition of the friction coefficient may cause numerical problems, therefore we use a smooth approximation (similar to the definition of tanh).

```
muAnisotropicSmooth = Function[{v, muDl, muDr},
   With[{s = 10}, (* s is a scaling factor that determines the
     sharpness of the step at 0, with larger s causing a sharper step *)
    (Exp[s v] - Exp[-s v]) / (Exp[s v] / (-muDr) - Exp[-s v] / (+muDl))]];
Plot[muAnisotropicSmooth[ v, 0.4, 0.6], {v, -10, 10}]
```

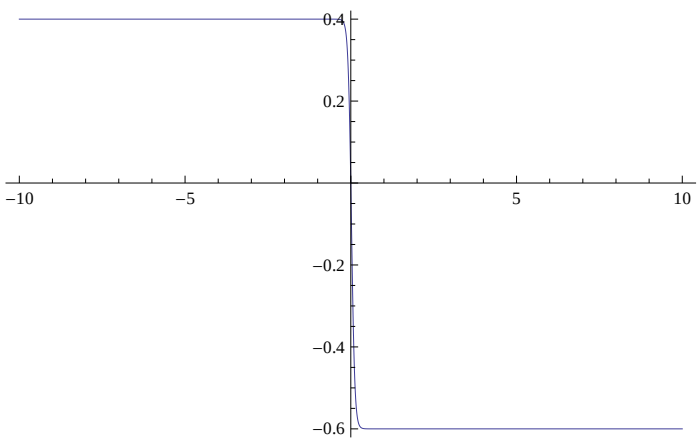

- **Operational Parameters**

Specify parameters that describe the simulation period: total simulation time, agitation frequency and amplitude.

```
tmax = 20;(* simulation time *)

(* agitation of substrate *)
fS = 0.5;(* frequency of vibration *)
aSx = 1; aSy = 1; aS = {aSx, aSy};(* amplitude of vibration *)
```

■ **Some Useful Agitation Functions**

A collection of commonly used agitation function, which can be selected simply by setting the corresponding number in the Switch statement.

```
{Sx, Sy} = Switch[2,
    1, {aSx Sin[2 Pi fS #] &, 0 &}, (* horizontal sine motion *)
    2, {0 &, aSy Sin[2 Pi fS #] &}, (* vertical sine motion *)
    3, {aSx Sawtooth[fS #] &, Sy = aSy 0 &}, (* horizontal sawtooth motion *)
    4, {aSx SawtoothSmooth[fS #] &, Sy = aSy 0 &},
    (* smooth horizontal sawtooth motion *)
    5, {aSx Sin[2 Pi fS #] Exp[-#] &, Sy = aSy 0 &}
    (* horizontal exponentially decaying sine motion *)
   ];
S = {Sx[#], Sy[#]} &;
Plot[S[t], {t, 0, tmax}];
ParametricPlot[S[t], {t, 0, tmax}];
DynamicModule[{t}, {Animator[Dynamic[t],
    {0, tmax}, AnimationDirection → Forward, AnimationRunning → False],
  Dynamic[ListPlot[{S[t]}, PlotMarkers → Automatic, AspectRatio → Automatic,
     PlotRange → {{-2 aSx, 2 aSx}, {-2 aSy, 2 aSy}}]]}]
```

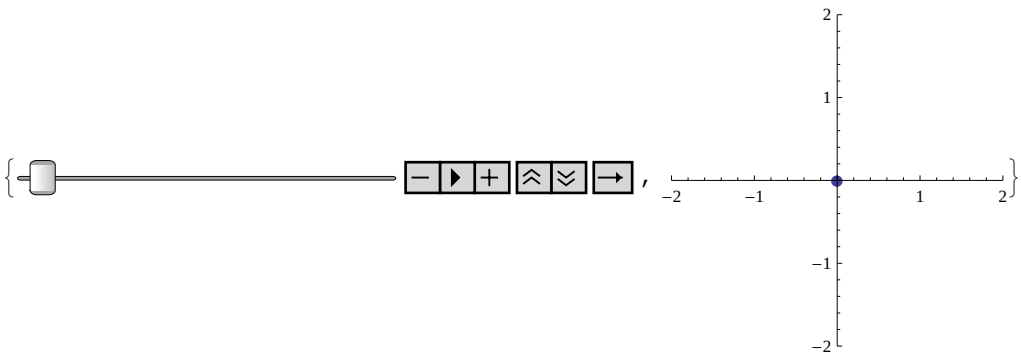

A Simple Model

Full 3-Point Model

The model consists of three point masses P, Q, and R. P represents the trailing edge, Q the leading edge, and R the center of mass. For now, P and Q are assumed always to be in contact with the substrate surface. Surface tension is represented by 3 springs between these 3 points. As the point masses move, they experience viscous damping and friction.

■ **System Parameters**

■ **Mass**

```
mP = 1; mQ = 1; mR = 5;(* point masses *)
```

■ **Viscous Damping**

```
b = 1;(* damping *)
(* NOTE: a better way to model damping might be to distinguish between
  damping during solid contact and damping during free motion in air *)
```

■ **Springs**

```
kPQ = 25; kQR = 20; kRP = 20;(* spring constants *)
lPQ = 8; lQR = 8; lRP = 8;(* spring lengths *)
```

■ **Friction Coefficients**

Both P (trailing edge) and Q (leading edge) experience anisotropic friction as they move along the substrate.

```
muDleftP = 9;(* advancing contact line at trailing edge (wetting) *)
(*leftP means when P is moving to the left*)
muDrightP = 1;(* receding contact line at trailing edge (dewetting) *)
muDleftQ = 6;(* receding contact line at leading edge (dewetting) *)
muDrightQ = 10;(* advancing contact line at leading edge (wetting) *)

(* wetting is less sensitive than dewetting *)
```

■ Forces Acting on Point Masses

The points P, Q, and R are functions of time. These functions are governed by a system of differential equations that derive from the sum of forces acting on them.

```
P = {Px[#], Py[#]} &; Q = {Qx[#], Qy[#]} &; R = {Rx[#], Ry[#]} &;
```

■ **Inertia**

```
(* inertial forces are due to gravity and acceleration: F = m g + m a *)
FinertiaPx = mP Gx - mP Px''[#] &; FinertiaPy = mP Gy - mP Py''[#] &;
FinertiaP = {FinertiaPx[#], FinertiaPy[#]} &;
FinertiaQx = mQ Gx - mQ Qx''[#] &; FinertiaQy = mQ Gy - mQ Qy''[#] &;
FinertiaQ = {FinertiaQx[#], FinertiaQy[#]} &;
FinertiaRx = mR Gx - mR Rx''[#] &; FinertiaRy = mR Gy - mR Ry''[#] &;
FinertiaR = {FinertiaRx[#], FinertiaRy[#]} &;
```

■ **Viscosity**

```
(* viscous forces are due to motion relative to a medium: F = -b (v - v_medium) *)
FviscosityPx = b (Qx'[#] - Px'[#]) + b (Rx'[#] - Px'[#]) &;
FviscosityPy = b (Qy'[#] - Py'[#]) + b (Ry'[#] - Py'[#]) &;
FviscosityP = {FviscosityPx[#], FviscosityPy[#]} &;
(* P is in contact with the substrate medium *)
FviscosityQx = b (Px'[#] - Qx'[#]) + b (Rx'[#] - Qx'[#]) &;
FviscosityQy = b (Py'[#] - Qy'[#]) + b (Ry'[#] - Qy'[#]) &;
FviscosityQ = {FviscosityQx[#], FviscosityQy[#]} &;
(* P is in contact with the substrate medium *)
FviscosityRx = b (Qx'[#] - Rx'[#]) + b (Px'[#] - Rx'[#]) &;
FviscosityRy = b (Qy'[#] - Ry'[#]) + b (Py'[#] - Ry'[#]) &;
FviscosityR = {FviscosityRx[#], FviscosityRy[#]} &;
(* P is in contact with the substrate medium *)
```

Elastic Springs

```
(* spring forces are due to elastic connections: F = -k (l - l_0) *)
FspringPx = kPQ (1 - lPQ / Norm[Q[#] - P[#]]) (Qx[#] - Px[#]) +
     kRP (1 - lRP / Norm[R[#] - P[#]]) (Rx[#] - Px[#]) &;
FspringPy = kPQ (1 - lPQ / Norm[Q[#] - P[#]]) (Qy[#] - Py[#]) +
     kRP (1 - lRP / Norm[R[#] - P[#]]) (Ry[#] - Py[#]) &;
FspringP = {FspringPx[#], FspringPy[#]} &;
FspringQx = kQR (1 - lQR / Norm[R[#] - Q[#]]) (Rx[#] - Qx[#]) +
     kPQ (1 - lPQ / Norm[P[#] - Q[#]]) (Px[#] - Qx[#]) &;
FspringQy = kQR (1 - lQR / Norm[R[#] - Q[#]]) (Ry[#] - Qy[#]) +
     kPQ (1 - lPQ / Norm[P[#] - Q[#]]) (Py[#] - Qy[#]) &;
FspringQ = {FspringQx[#], FspringQy[#]} &;
FspringRx = kRP (1 - lRP / Norm[P[#] - R[#]]) (Px[#] - Rx[#]) +
     kQR (1 - lQR / Norm[Q[#] - R[#]]) (Qx[#] - Rx[#]) &;
FspringRy = kRP (1 - lRP / Norm[P[#] - R[#]]) (Py[#] - Ry[#]) +
     kQR (1 - lQR / Norm[Q[#] - R[#]]) (Qy[#] - Ry[#]) &;
FspringR = {FspringRx[#], FspringRy[#]} &;
```

Friction

```
(* friction forces are due to sliding motion: F = - mu F_normal sign(v) *)
FfrictionPx = (-mP Gy) muAnisotropicSmooth[Px'[#] - Sx'[#], muDleftP, muDrightP] &;
FfrictionPy = 0 &; FfrictionP = {FfrictionPx[#], FfrictionPy[#]} &;
(* NOTE: here I assume incorrectly that F_normal = m g; however,
this may be a reasonably accurate model for pinning forces *)
FfrictionQx = (-mQ Gy) muAnisotropicSmooth[Qx'[#] - Sx'[#], muDleftQ, muDrightQ] &;
FfrictionQy = 0 &; FfrictionQ = {FfrictionQx[#], FfrictionQy[#]} &;
(* NOTE: here I assume incorrectly that F_normal = m g; however,
this may be a reasonably accurate model for pinning forces *)
FfrictionRx = 0 &; FfrictionRy = 0 &;
FfrictionR = {FfrictionRx[#], FfrictionRy[#]} &;
(* R is not in contact with the substrate *)
```

Normal Force

The normal force is provided by the initial substrate surface. We do not know this force a priori, it balances the combined forces that the point applies to the surface.
NOTE: this force is currently not explicitly used in our equations. Rather, for a point that is constrained to be in contact with the substrate, we just relax the force balance condition and assume that the normal force has the right magnitude to keep the point on the surface.

```
(* normal forces are due to the contact with a solid surface *)
(* they are assumed to be equal to gravity *)
FnormalPx = 0 &; FnormalPy = -mP Gy &;
FnormalP = {FnormalPx[#], FnormalPy[#]} &;
FnormalQx = 0 &; FnormalQy = -mQ Gy &;
FnormalQ = {FnormalQx[#], FnormalQy[#]} &;
FnormalRx = 0 &; FnormalRy = -mR Gy &;
FnormalR = {FnormalRx[#], FnormalRy[#]} &;
```

■ **Total Force**

```
(* the total force is the sum of all the components above *)
FPx = FinertiaPx[#] + FviscosityPx[#] + FspringPx[#] + FfrictionPx[#] + FnormalPx[#] &;
FPy = FinertiaPy[#] + FviscosityPy[#] + FspringPy[#] + FfrictionPy[#] + FnormalPy[#] &;
FP = {FPx[#], FPy[#]} &;
FQx = FinertiaQx[#] + FviscosityQx[#] + FspringQx[#] + FfrictionQx[#] + FnormalQx[#] &;
FQy = FinertiaQy[#] + FviscosityQy[#] + FspringQy[#] + FfrictionQy[#] + FnormalQy[#] &;
FQ = {FQx[#], FQy[#]} &;
FRx = FinertiaRx[#] + FviscosityRx[#] + FspringRx[#] + FfrictionRx[#] + FnormalRx[#] &;
FRy = FinertiaRy[#] + FviscosityRy[#] + FspringRy[#] + FfrictionRy[#] + FnormalRy[#] &;
FR = {FRx[#], FRy[#]} &;
```

■ Equations of Motion

The motions of the point P, Q, and R are given by finding functions P(t), Q(t), and R(t) that satisfy the force equations above such that at each point, the forces balance out. This leads to a system of differential equations.

■ **Dynamics**

The dynamics are governed by the condition that the sum of forces at each point has to be zero, unless there is a geometric constraint on the point (such as, e.g., “stay in contact with the moving substrate”).

```
Dyn = {FPx[t] == 0, (*FPy[t]==0,*)FQx[t] == 0, (*FQy[t]==0,*)FRx[t] == 0, FRy[t] == 0};
```

■ **Geometric Constraints**

The interplay between drop and substrate surface may lead to additional geometric conditions.

```
Constraints = {Py[t] == Sy[t], Qy[t] == Sy[t]}; (*P and Q touch the surface always*)
```

■ **Initial Conditions**

```
Init = {Px[0] == 2, Px'[0] == 0, Py[0] == 0, Py'[0] == 0,
    Qx[0] == 10, Qx'[0] == 0, Qy[0] == 0, Qy'[0] == 0,
    Rx[0] == 6, Rx'[0] == 0, Ry[0] == Sqrt[64 - 16], Ry'[0] == 0};
(*In this case, the drop is under compression due to gravity*)
```

Solution of Differential Equations of Motion

```
Eqs = Join[Dyn, Constraints, Init];
Sol = First[NDSolve[Eqs, {Px, Py, Qx, Qy, Rx, Ry}, {t, 0, tmax}]];
Plot[Evaluate[{Px[t](*-Px[0]*), Qx[t](*-Qx[0]*), Rx[t](*-Rx[0]*)} /. Sol],
 {t, 2, tmax}, AxesLabel → {"Time", "Displacement"},
 PlotLegend → {"P: Trailing edge", "Q: Leading edge", "R: Center of mass"},
 PlotStyle → {Directive[Red, Thick], Directive[Blue, Thick], Directive[Green, Thick]},
 AxesStyle → 20, RotateLabel → False]
ParametricPlot[{(*P[t],Q[t],*)R[t]} /. Sol, {t, 0, tmax},
  PlotRange → All, AspectRatio → Full, AxesLabel → {"x", "y"}];
ParametricPlot[Evaluate[{P[t], Q[t], R[t]} /. Sol], {t, 0, tmax},
 PlotRange → All, (*sAspectRatio→Full,*)AxesLabel → {"x", "y"}]
Plot[FPy[t] /. Sol, {t, 0, tmax}, AxesLabel → {"t", "FPy(t)"}];
TEMP = DynamicModule[{t}, {Animator[Dynamic[t], {0, tmax},
    AnimationDirection → Forward, AnimationRunning → True], Dynamic[
    ListLinePlot[Evaluate[{P[t], Q[t], R[t], P[t]} /. Sol], PlotMarkers → Automatic,
     AspectRatio → Automatic, PlotRange → {{-5, 20}, {-5, 20}}]
    (*PlotEllipse[Evaluate[P[t]/.Sol],Evaluate[Q[t]/.Sol],Evaluate[R[t]/.Sol]]*)
   ]}]
Export["file.txt",
 Evaluate[{Px[t](*-Px[0]*), Qx[t](*-Qx[0]*), Rx[t](*-Rx[0]*)} /. Sol]]
Export["animation.gif", TEMP]
```

```
animation.gif
```

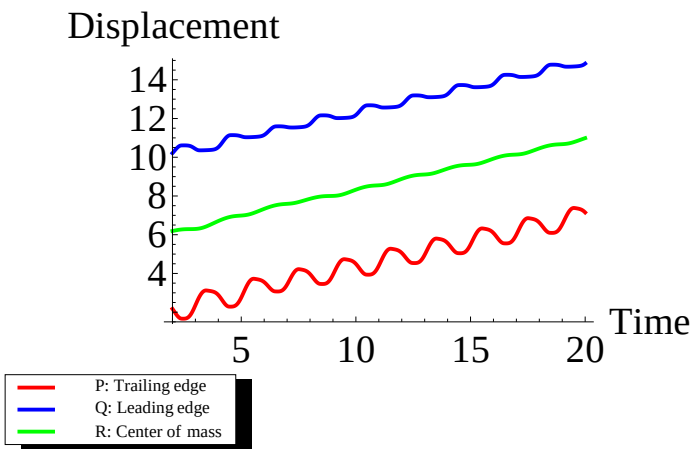

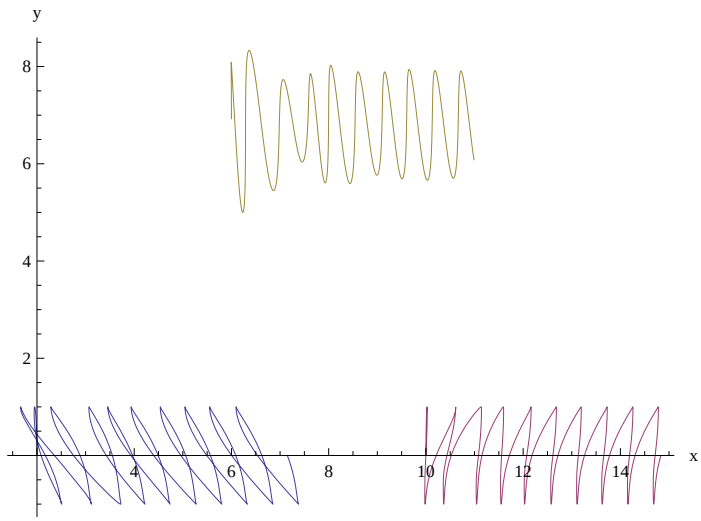

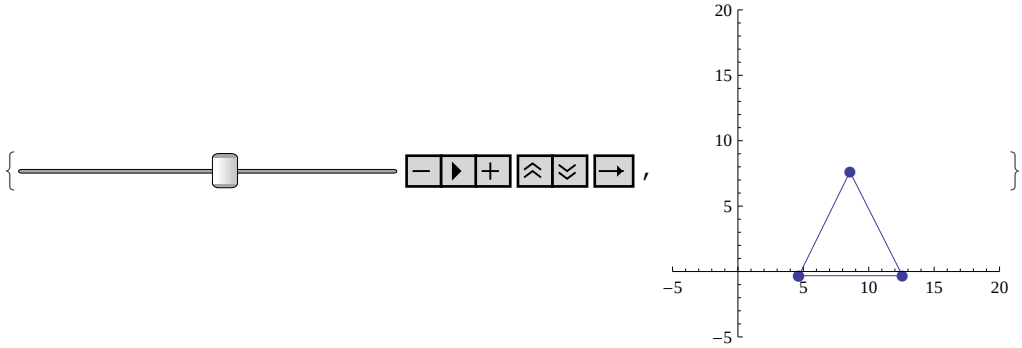

file.txt

Acknowledgements

The author wishes to express sincere appreciation to the Department of Bioengineering for their extended long-term support, especially to Professor Karl Böhringer for his vast reserve of patience and knowledge, and to Professor Gerald Pollack for his intriguing advices throughout the program. This thesis would never have been completed without the encouragement and devotion of my lab mates, family and friends. Especially, I want to give special thanks to my dearest wife, Beibei Chen, whose patient love and support enables me to complete this work.